PSYCHIATRIC DISEASES

Distinct neural mechanisms for the prosocial and rewarding properties of MDMA

Boris D. Heifets[1,2], Juliana S. Salgado[1,2], Madison D. Taylor[2], Paul Hoerbelt[2], Daniel F. Cardozo Pinto[2], Elizabeth E. Steinberg[2], Jessica J. Walsh[2], Ji Y. Sze[3], Robert C. Malenka[2]*

The extensively abused recreational drug (±)3,4-methylenedioxymethamphetamine (MDMA) has shown promise as an adjunct to psychotherapy for treatment-resistant psychiatric disease. It is unknown, however, whether the mechanisms underlying its prosocial therapeutic effects and abuse potential are distinct. We modeled both the prosocial and nonsocial drug reward of MDMA in mice and investigated the mechanism of these processes using brain region–specific pharmacology, transgenic manipulations, electrophysiology, and in vivo calcium imaging. We demonstrate in mice that MDMA acting at the serotonin transporter within the nucleus accumbens is necessary and sufficient for MDMA's prosocial effect. MDMA's acute rewarding properties, in contrast, require dopaminergic signaling. MDMA's prosocial effect requires 5-HT1b receptor activation and is mimicked by *d*-fenfluramine, a selective serotonin-releasing compound. By dissociating the mechanisms of MDMA's prosocial effects from its addictive properties, we provide evidence for a conserved neuronal pathway, which can be leveraged to develop novel therapeutics with limited abuse liability.

INTRODUCTION

(±)3,4-Methylenedioxymethamphetamine (MDMA) is an extensively used and often abused drug that has addictive liability and toxic side effects (*1*). Yet, at modest doses, it has the well-documented and potentially therapeutic effects of enhancing feelings of trust, emotional openness, and perhaps empathy (*2*, *3*, *4*). Despite the potential negative consequences of MDMA ingestion, because of its profound prosocial effects, MDMA is being evaluated to determine its efficacy in the treatment of posttraumatic stress disorder and autism spectrum disorders (*4*, *5*). However, it is unknown whether the mechanisms underlying MDMA's prosocial, therapeutic effect and abuse potential can be separated (*1*), a topic with important implications for the future therapeutic use of MDMA as well as for the development of similar agents with less potential morbidity.

MDMA is a substituted amphetamine with high affinity for the serotonin [5-hydroxytryptamine (5-HT)] and dopamine (DA) transporters (SERT and DAT, respectively) (*6*, *7*), through which it stimulates release of these neurotransmitters. MDMA's acute reinforcing effects, which strongly predict addictive liability (*8*, *9*), have been linked to its DA-releasing properties (*10*, *11*, *12*), whereas the role of SERT in this action is uncertain (*13*, *14*). Studies on the detailed mechanisms underlying the prosocial effects of MDMA are confusing and implicate several different neuromodulatory substances including 5-HT, DA, and oxytocin (Oxt) (*1*, *3*, *12*). Recent work highlights the role of serotonergic signaling in social approach behaviors, particularly within the nucleus accumbens (NAc) (*15*, *16*), a conserved brain region that regulates appetitive behavior. We therefore hypothesized that MDMA's interaction with SERT specifically in the NAc could fully account for MDMA's prosocial effect but not its rewarding effect. We modeled MDMA's acute prosocial and nonsocial rewarding effects in mice. Using complementary genetic and brain region–specific pharmacological manipulations, and in vivo calcium imaging, we found that MDMA acts at SERT-containing 5-HT terminals in the NAc. MDMA's nonsocial rewarding effect does not require SERT but rather involves dopaminergic signaling in the NAc. Convergent evidence from behavioral pharmacology and electrophysiology experiments further demonstrates that MDMA's prosocial effect requires activation of the 5-HT1b receptor in the NAc and does not require Oxt receptor (OxtR) signaling. Last, we found that MDMA's prosocial effect can be mimicked by *d*-fenfluramine (FEN), a selective serotonin-releasing drug with limited abuse liability in humans.

RESULTS

MDMA produces both prosocial behavior and nonsocial reward in mice

To study the prosocial effects of MDMA, we used the three-chamber social approach assay (Fig. 1A) (*17*). MDMA dose-dependently increased the time a free mouse explores the chamber containing an age- and sex-matched conspecific stranger mouse kept in an enclosure that allows physical interaction (Fig. 1B, fig. S1A, and table S1). At its lowest effective dose (7.5 mg/kg), the greatest effect of MDMA occurred in the final 10 min of the session, at a time when saline-treated mice consistently showed a neutral social preference (Fig. 1, C and D, and table S1); therefore, we quantified this epoch in all subsequent experiments using a "sociability index" (see Materials and Methods). Whereas the enhancement of social approach was greatest when both mice received MDMA, a clear enhancement of social preference still occurred when only the free mouse received MDMA (Fig. 1E and table S1). Furthermore, MDMA had equal prosocial effects in both male and female mice (fig. S1B and table S1) and still caused increased preference for a live mouse compared to a toy mouse placed in the other enclosure (fig. S1C and table S1).

We also tested whether MDMA has a similar effect on approach versus avoidance behavior in a nonsocial context, using the elevated plus maze. In contrast to anxiolytics, such as benzodiazepine class drugs (*18*), MDMA increased neither the number of visits nor the

[1]Department of Anesthesiology, Perioperative and Pain Medicine, Stanford University School of Medicine, Stanford, CA 94305, USA. [2]Nancy Pritzker Laboratory, Department of Psychiatry and Behavioral Sciences, Stanford University, Stanford, CA 94305, USA. [3]Department of Molecular Pharmacology and Rose F. Kennedy Intellectual and Developmental Disabilities Center, Albert Einstein College of Medicine, Bronx, NY 10461, USA.
*Corresponding author. Email: malenka@stanford.edu

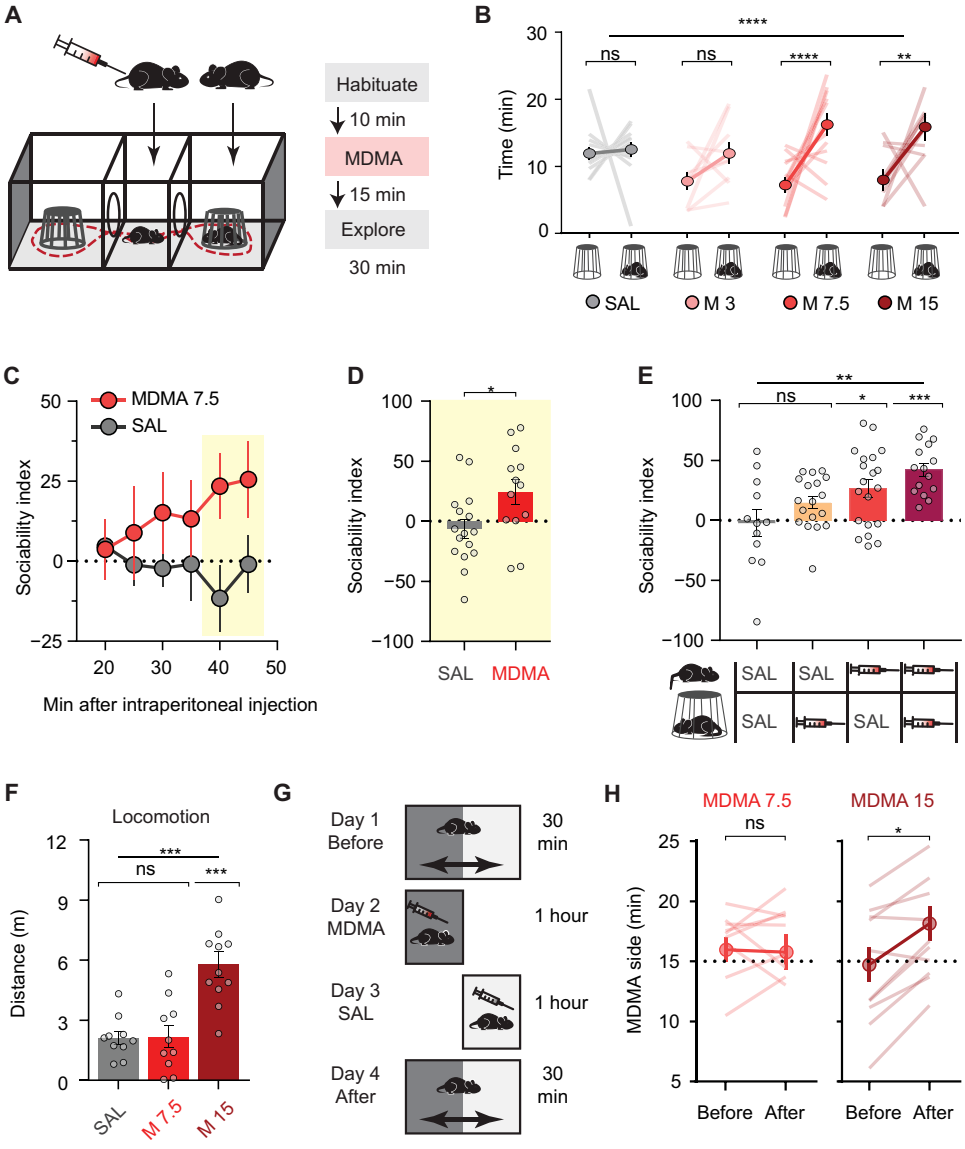

Fig. 1. MDMA enhances social preference in mice. (**A**) Three-chamber social interaction assay schematic with experimental timeline. (**B**) Time spent with "mouse cup" versus "empty cup" after increasing doses of MDMA ($n = 9$ to 13). SAL, saline; ns, not significant. (**C**) Time course of social preference during 30-min exploration after lowest effective dose of MDMA (7.5 mg/kg) compared to saline treatment ($n = 14$ to 16). Yellow box indicates the time of maximal MDMA effect. (**D**) Summary of sociability index in final 10 min. (**E**) MDMA's prosocial effect as a function of mice receiving MDMA or saline injections ($n = 12$ to 20). (**F**) Locomotor activity after either saline, the lowest effective dose of MDMA in the three-chamber assay (7.5 mg/kg), or a higher dose of MDMA (15 mg/kg; $n = 10$ to 11). (**G**) Conditioned place preference (CPP) schematic using a single 1-hour pairing of context with MDMA. (**H**) Preference for MDMA-paired side, before and after conditioning ($n = 10$ to 11). CPP data is shown after low-dose (left) and higher-dose MDMA (right). Data shown are means ± SEM. Significance was determined for each comparison (statistical test): across groups (one-way ANOVA, unmatched) for (B), (E), and (F); across group time courses (two-way ANOVA, ordinary) for (C); between groups (unpaired t test) for (D); within group (paired t test) for (H); all planned post hoc between-group comparison (t test with Sidak correction for multiple comparisons). *$P < 0.05$, **$P < 0.01$, ***$P < 0.001$, and ****$P < 0.0001$; ns, $P > 0.05$.

time spent in the open arms of the maze (fig. S1, D to G, and table S1), consistent with prior studies (*6*). Thus, MDMA appears to preferentially enhance exploration of social targets. We hypothesized that if MDMA engages distinct neural circuitry for social approach versus drug reward, then these effects may emerge at different doses. The lowest dose of MDMA that reliably elicits prosocial behavior (7.5 mg/kg) had no locomotor stimulant activity (Fig. 1F and table S1) and did not cause a conditioned place preference (CPP) with either one or two drug-context pairings (Fig. 1, G and H, fig. S1, H and I, and table S1). A single higher dose of MDMA (15 mg/kg), however, produced both behaviors (Fig. 1, F and H, and table S1), which strongly correlate with a drug's addictive liability (*8*, *9*) and parallels the psychomotor activation and drug "liking" associated with MDMA use in humans (*1*). Single doses of varying size can thus separate prosocial behavior from drug reward, allowing us to study the respective mechanisms of MDMA's acute behavioral effects without the confounding effects of behavioral plasticity that may accompany multiple-dose regimens.

MDMA's prosocial effect requires SERT

Several neuromodulatory systems have been implicated in MDMA's behavioral effects, including 5-HT, DA, and Oxt (*1*, *3*, *6*, *12*), all of which have been suggested to play roles in both social behavior and addiction (*9*, *15*, *16*, *19*). The highest affinity binding of MDMA is to SERT (*6*, *7*) leading to supraphysiological 5-HT release through a reverse-transport mechanism (*20*, *21*, *22*). To test whether this interaction is required for MDMA's prosocial effects, we pretreated subjects with the selective serotonin reuptake inhibitor (SSRI) (S)-citalopram (SCIT). SCIT binds to SERT and thereby inhibits MDMA binding but alone does not cause large increases in 5-HT (*21*). Although SCIT treatment alone did not alter social preference, it prevented the increase in social approach normally elicited by MDMA (Fig. 2A and table S2). These data highlight the difference in magnitude of the expected increase in 5-HT concentration due to reverse transport versus reuptake inhibition: The former is associated with constitutive neurotransmitter release resulting in high concentrations of 5-HT at synapses, independent of action-potential activity (*21*); the latter is related to neuronal activity (*23*).

To independently and more directly test the importance of SERT in mediating MDMA's prosocial effect, we injected SERT conditional knockout (cKO) mice ($SERT^{fl/fl}$) (Fig. 2B) with a Cre recombinase–expressing adeno-associated virus (AAV-Cre) into the dorsal raphe (DR), a major 5-HTergic brain nucleus (Fig. 2C). This manipulation

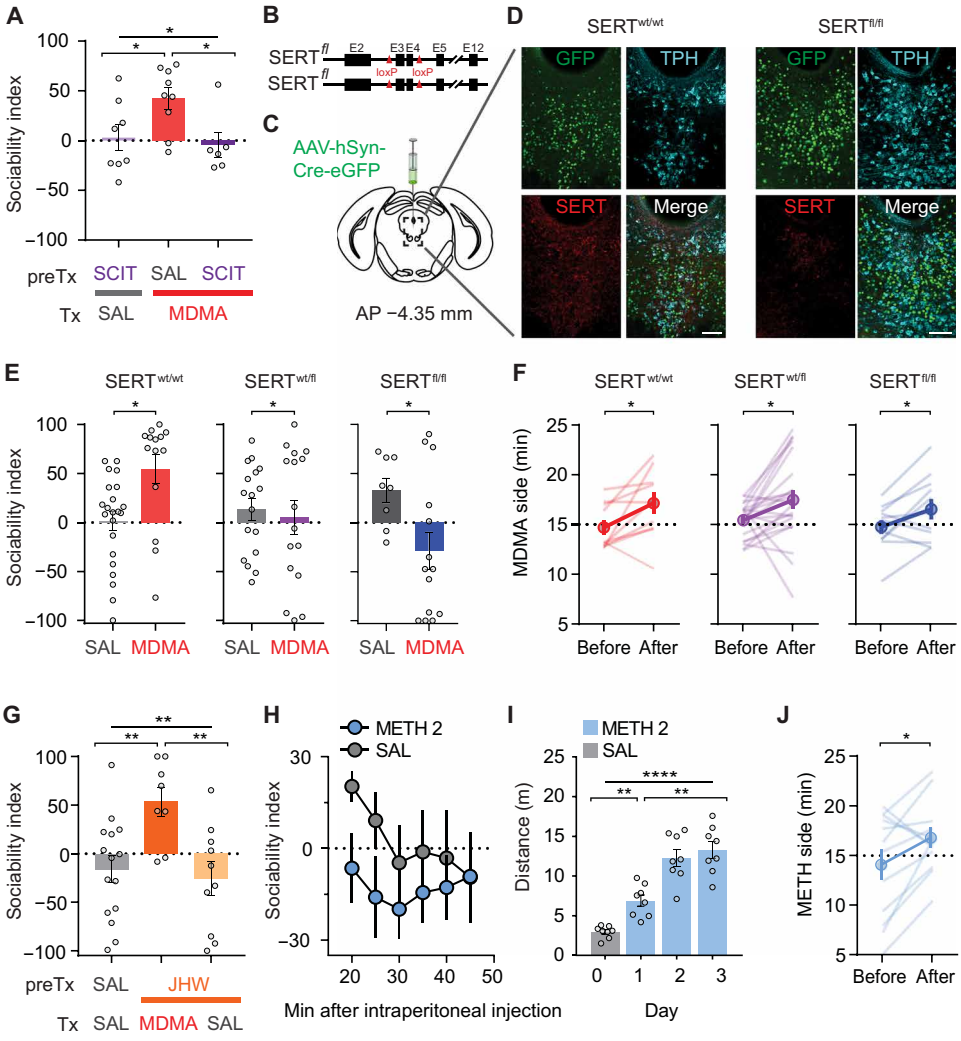

Fig. 2. MDMA's interaction with SERT accounts for its prosocial, but not its rewarding, effects. (**A**) Sociability in mice pretreated (preTx) with saline or the SSRI, SCIT, before treatment (Tx) with MDMA or saline. Saline + MDMA group is compared to SCIT + saline and SCIT + MDMA groups ($n = 6$ to 9). (**B**) Schematic of SERT cKO mouse, which has exons 3 and 4 floxed. (**C**) Schematic of AAV containing Cre-eGFP injected into the DR of adult $SERT^{wt/wt}$, $SERT^{fl/wt}$, and $SERT^{fl/fl}$ mice. (**D**) Sample images of immunohistochemistry of Cre-eGFP–injected DR from a wild-type mouse and $SERT^{fl/fl}$ littermate; coronal brain section represents area enclosed by dashed box in (C). 5-HTergic cells visualized by tryptophan hydroxylase (TPH). (eGFP, green; anti-SERT, red; anti-TPH2, cyan; scale bars, 100 μm). (**E**) Sociability after MDMA (7.5 mg/kg) in Cre-eGFP–injected wild-type mice and in heterozygous and homozygous SERT cKO mice ($n = 8$ to 22). (**F**) CPP data after high-dose MDMA (15 mg/kg) in all three groups of mice from (E) ($n = 11$ to 22). Preference for MDMA-paired side is shown before and after conditioning. (**G**) Sociability in mice pretreated with saline or a selective DAT inhibitor, JHW-007 (10 mg/kg), before treatment with MDMA or saline. JHW + MDMA group is compared to saline + saline, and JHW + saline groups ($n = 8$ to 15). (**H**) Time course of sociability index after METH administration (2 mg/kg) versus saline (SAL; $n = 9$ to 10). (**I**) Locomotor sensitization after METH (2 mg/kg) is given on successive days ($n = 8$). (**J**) Preference for METH-paired side in a CPP assay (J; $n = 12$). Data shown are means ± SEM. Significance was determined for each comparison (statistical test): across groups (one-way ANOVA, unmatched) for (A) and (G); between groups (unpaired *t* test) for (E); within group (paired *t* test) for (F) and (J); across group time courses (two-way ANOVA, ordinary) for (H); within group time course (one-way ANOVA, repeated measures) for (I); all planned post hoc between-group comparison (*t* test with Sidak correction for multiple comparisons). $^*P < 0.05$, $^{**}P < 0.01$, and $^{****}P < 0.0001$; ns, $P > 0.05$.

markedly reduced SERT staining in the DR (Fig. 2D, fig. S2, and table S2) and prevented MDMA's prosocial effect in heterozygous $SERT^{fl/wt}$ mice (Fig. 2E and table S2). Homozygous $SERT^{fl/fl}$ mice that had received DR AAV-Cre injections displayed an apparent social aversion in response to MDMA, compared to the saline-treated group (Fig. 2E and table S2). In marked contrast to these findings, we observed MDMA-induced CPP in wild-type mice as well as heterozygous and homozygous SERT cKO mice, indicating that genetic deletion of SERT from DR neurons does not influence MDMA-induced CPP (Fig. 2F and table S2).

MDMA's prosocial effect does not require DAT-driven DA release

Because MDMA also releases DA via reverse transport due to binding at DAT (*22*, *24*, *25*), we next examined whether DAT is required for MDMA's prosocial action. Pretreating subjects with the atypical DAT inhibitor JHW-007, which prevents cocaine's behavioral effects (*26*), did not influence MDMA's prosocial effect (Fig. 2G and table S2). Next, we tested methamphetamine (METH), which is structurally related to MDMA and releases DA due to high affinity for DAT but does not interact with SERT (*7*). METH (2 mg/kg) had no prosocial effect (Fig. 2H and table S2) but did generate both locomotor sensitization (Fig. 2I and table S2) and CPP (Fig. 2J and table S2), indicating that METH at this dose was indeed behaviorally active. These results demonstrate that the MDMA- and METH-elicited behaviors that correlate with addiction (*8*, *9*) are largely due to DAT binding and the consequent increase in DA release. In contrast, all results thus far suggest that the prosocial effect of MDMA only requires binding to SERT, not DAT.

MDMA's prosocial effect is due to action at 5-HT terminals in NAc

Where in the brain does MDMA act to elicit its prosocial effect? Because increasing 5-HT release in the NAc promotes sociability (*16*), we hypothesized that MDMA's interaction with SERT specifically in the NAc could fully account for MDMA's prosocial effect. Consistent with this prediction, infusing SCIT bilaterally into the NAc blocked the prosocial effect of systemic MDMA (Fig. 3A, fig. S3A, and table S3), whereas infusion of SCIT into the ventral tegmental area (VTA), which receives dense DR 5-HT innervation (*27*), had no effect on this behavioral action of MDMA (Fig. 3B, fig. S3B, and table S3). Furthermore, direct intra-NAc infusion of MDMA produced a prosocial effect comparable to that elicited by systemic MDMA administration (Fig. 3C and table S3). In contrast,

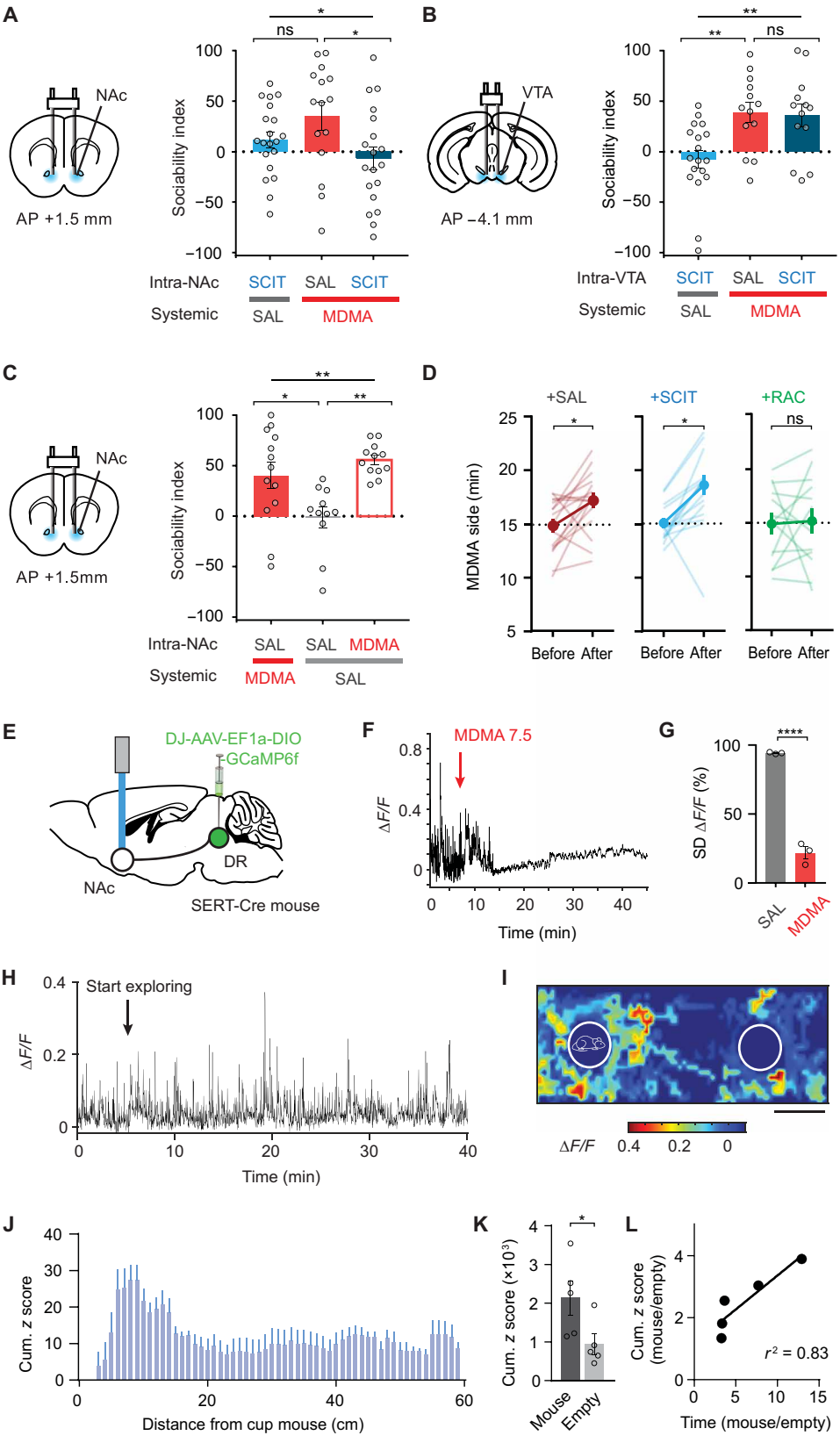

Fig. 3. MDMA's prosocial, but not its rewarding, effect requires interaction with SERT in NAc. (**A**) Left: Schematic of drug infusion into the NAc. Right: Sociability in mice pretreated with saline or SCIT infused into the NAc before intraperitoneal treatment with MDMA or saline. Saline-NAc + MDMA-intaperitoneal is compared to SCIT-NAc + saline-intraperitoneal and SCIT-NAc + MDMA intraperitoneal groups. $n = 15$ to 20. (**B**) Left: Schematic of drug infusion into the VTA. Right: Sociability in mice pretreated with saline or SCIT infused into the VTA before intraperitoneal treatment with MDMA or saline. Saline-VTA + MDMA-intraperitoneal is compared to SCIT-VTA + saline-intraperitoneal and SCIT-VTA + MDMA intraperitoneal groups. $n = 13$ to 18. (**C**) Left: Schematic as in (A). Right: Sociability in mice pretreated with saline or MDMA infused into the NAc before intraperitoneal treatment with MDMA or saline. Saline-NAc + saline-intraperitoneal is compared to saline-NAc + MDMA-intaperitoneal and MDMA-NAc + saline intraperitoneal groups ($n = 11$ to 13). (**D**) CPP data after MDMA (15 mg/kg) in mice pretreated with either saline, SCIT, or the D2R antagonist raclopride (RAC) infused into the NAc ($n = 13$ to 16). (**E**) Schematic of fiber photometry experiments. GCaMP6f was expressed in DR 5-HT neurons to allow imaging of their projections within the NAc during the three-chamber assay. (**F** and **G**) GCaMP6f fluorescence from SERT-expressing neurons terminals in the NAc after MDMA (7.5 mg/kg). (F) Sample trace. Arrow denotes intraperitoneal MDMA injection. (G) Summary graph of SD of $\Delta F/F$ during 5-min epoch after either saline (SAL) or MDMA (7.5 mg/kg), normalized to SD of $\Delta F/F$ during the 5 min before injection ($n = 3$). (**H**) Sample trace illustrating GCaMP6f transients from SERT+ terminals in the NAc during three-chamber exploration. (**I**) Spatial heat map example. The maximal $\Delta F/F$ occurring for each explored area of the three-chamber apparatus is shown for one 30-min session. Outlines of mouse cup (left) and empty cup (right) are drawn. (**J**) Summary graph of z-scored fluorescence as a function of distance from the mouse cup. (**K**) Summary graph of cumulative z-scored fluorescence for the area around the mouse cup versus empty cup ($n = 5$ mice). (**L**) Ratio of mouse cup to empty cup–related GcaMP6f fluorescence as function of the ratio of time spent in the same two areas. Data shown are means ± SEM. Significance was determined for each comparison (statistical test): across groups (one-way ANOVA, unmatched) for (A) to (C); within group (paired t test) for (D); between groups (unpaired t test) for (G) and (K); univariate correlation (linear regression) for (L); all planned post hoc between-group comparison (t test with Sidak correction for multiple comparisons). $^*P < 0.05$, $^{**}P < 0.01$, and $^{****}P < 0.0001$; ns, $P > 0.05$.

intra-NAc SCIT had no effect on MDMA-induced CPP, which was fully blocked by the DA type 2 receptor (D2R) antagonist, raclopride (Fig. 3D and table S3) (*10*, *11*). These results suggest that MDMA acting solely on SERT in NAc 5-HT terminals accounts for its prosocial effects.

To further test this hypothesis, we expressed the fluorescent calcium indicator, GCaMP6f, in DR 5-HT neurons and recorded fluorescence changes in 5-HT fibers in the NAc during administration of MDMA (Fig. 3, E to G, and fig. S3C). MDMA binding to SERT causes reverse transport of 5-HT and collapse of the normal pH gradient between 5-HT synaptic vesicles and the cytoplasm (*20*). Because GCaMP6f fluorescence is pH sensitive (*28*), by acidifying terminals upon which it acts (*20*), MDMA should quench this fluorescence. Consistent with this prediction, systemic MDMA administration caused a rapid, large reduction of GCaMP6f fluorescence in DR 5-HT inputs in NAc (Fig. 3, F and G, and table S3). In the absence of MDMA, activity in NAc 5-HT inputs increased when the free test mouse approached the "cup" mouse in a manner that inversely correlated with their distance apart (Fig. 3, H to K, and table S3). In addition, the magnitude of this increase correlated with the degree of social preference exhibited by the test mouse (Fig. 3L and table S3). These findings provide further evidence that activity in DR 5-HT inputs in the NAc encodes some component of social preference, and MDMA acts directly on these inputs.

To determine whether MDMA's effect on NAc physiology mimics that of 5-HT (*15*, *23*), as predicted by our hypothesis, we performed whole-cell voltage-clamp recordings from visually identified NAc medial shell D1R and D2R expressing medium spiny neurons (MSNs) in acute brain slices and bath-applied MDMA while stimulating excitatory inputs (Fig. 4, A to C). MDMA (10 μM) precisely mimicked the actions of 5-HT in that it elicited a long-term depression (LTD) of excitatory postsynaptic currents (EPSCs) in both D1 and D2 MSNs (Fig. 4, B and C, and table S4).

NAc 5-HT1b receptors, but not OxtRs, are required for MDMA's prosocial effect

MDMA's effects on social interactions and its effect on synaptic transmission in the NAc have been suggested to involve Oxt (*3*, *29*), a neuropeptide that plays important roles in a variety of social behaviors (*19*). In particular, a recent study that appeared during the revision of this paper found that sensitivity to social reward in mice, which declines with age, could be reestablished after a single dose of MDMA administered 6 hours to 2 weeks before behavioral testing (*29*). This delayed effect of MDMA was blocked by pretreatment with an OxtR antagonist and was attributed to MDMA-evoked Oxt release in the NAc. Prior work using the same behavioral assay suggested that social reward is mediated by OxtR-triggered 5-HT release in the NAc, with subsequent 5-HT1b receptor activation (*15*). To clarify the upstream/downstream relationship of OxtR activation and 5-HT release in the NAc, we assayed OxtR and 5HTR1b receptor involvement in MDMA's acute prosocial effect and MDMA's effect on synaptic transmission in the NAc. Pretreating mice with the OxtR antagonist L-368,899 at a dose (5 mg/kg) that blocks Oxt-dependent behaviors (*15*, *30*) had no effect on MDMA-induced sociability (Fig. 4D and table S4). Higher or repeated systemic doses of L-368,899 or intra-NAc infusion of either L-368,899 or the more selective and potent OxtR antagonist, L-371,257, also had no influence on MDMA's prosocial effect (Fig. 4, D and E, and table S4). Furthermore, MDMA still produced its normal prosocial effect in mice in which OxtRs were genetically deleted in 5-HT neurons by crossing the $OxtR^{fl/fl}$ mouse line with the SERT-Cre mouse line (Fig. 4F and table S4).

Last, we tested whether an OxtR antagonist could block the effect of a low dose of MDMA (2 μM) on excitatory synaptic transmission in the NAc, as recently reported (*29*). We found that applying this low dose of MDMA to brain slices transiently depressed EPSCs in NAc MSNs but did not result in LTD. This synaptic effect of MDMA was unaffected by incubating slices with the OxtR antagonist, L-368,899 at a concentration (5 μM) that prevents the LTD induced by application of Oxt (fig. S4, A and B, and table S4) (*15*). These findings provide evidence that OxtRs are not required for the acute prosocial effect of MDMA and are consistent with previous findings that Oxt release in the NAc promotes social reward by increasing 5-HT release (*15*). We next tested whether, like the actions of 5-HT in the NAc (*16*), MDMA's prosocial effect and MDMA-LTD in NAc brain slices are 5-HT1b receptor dependent. Intra-NAc infusion of the 5-HT1b receptor antagonist NAS-181 in vivo blocked MDMA's prosocial effect (Fig. 4G and table S4), and prior application of NAS-181 to brain slices prevented the LTD induced by MDMA (10 μM) (Fig. 4, H and I, and table S4), indicating that the behavioral and electrophysiological effects of MDMA-evoked 5-HT release require activation of NAc 5-HT1b receptors.

A 5-HT releasing drug mimics MDMA's prosocial effect

A role for 5-HT release and specific 5-HT receptor subtypes in mediating MDMA's prosocial effect has previously been suggested (*3*). However, this work did not address the locus of MDMA's action nor did it define if the mechanisms mediating MDMA's acute reinforcing effect are the same as those mediating its effects on sociability. Our demonstration that MDMA's addictive liability appears to be due entirely to its DA-releasing properties predicts that a drug that mechanistically functions like MDMA but binds only to SERT and not DAT should have the same prosocial effect with no acute reinforcing properties. FEN exhibits these properties (*7*) and, importantly, has no acute reinforcing effect when tested in multiple species (*7*, *31*). We therefore examined FEN and found that, like MDMA, it enhanced social preference dose dependently (Fig. 4, J and K, and table S4) and generated an identical electrophysiological signature (Fig. 4L and table S4).

DISCUSSION

The importance of our conclusions for understanding the mechanisms mediating MDMA's unique prosocial actions in humans depends on the assumption that the neural mechanisms we have elucidated in mice reflect those mediating MDMA's actions in the human brain. Several lines of evidence support this assumption. First, the consistent, robust effects of MDMA in the three-chamber assay parallel the prosocial effect that is central to the human experience. Second, at higher doses, MDMA's psychomotor stimulant and acute reinforcing actions predict addictive liability (*8*, *9*), which has been documented in human MDMA abusers (*1*). Third, human pharmacology experiments suggest that aspects of MDMA's subjective effects are sensitive to both an SSRI and D2R antagonist (*12*), findings that mimic our more precise manipulations in mice. Fourth, the prosocial effects of Oxt administration in humans are qualitatively different from those of MDMA (*3*), consistent with the lack of a role for Oxt in mediating MDMA's acute prosocial effects in our assays.

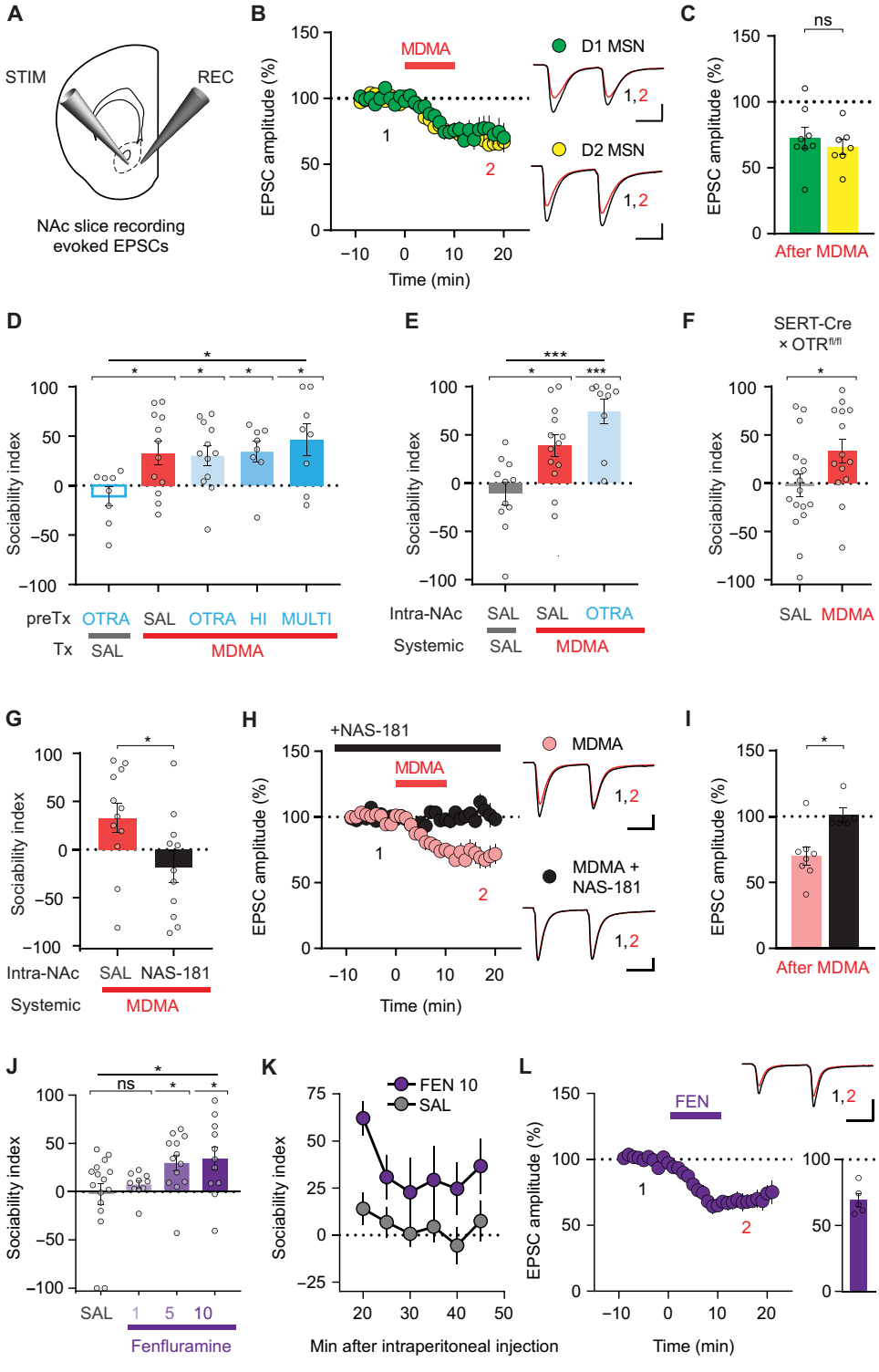

Fig. 4. MDMA's prosocial effect requires 5-HT release and activation of 5-HT1b receptors in NAc. (**A**) Schematic for slice electrophysiology from coronal brain slices containing NAc. (**B**) Left: Summary time course graph showing the effect of a 10-min bath application of MDMA (10 μM) on EPSC amplitudes recorded from D1 and D2 MSNs. Right, sample EPSC traces taken from time points 1 and 2 as shown. (**C**) Summary graph shows EPSC amplitudes in D1 and D2 MSNs after MDMA application (n = 7 to 8 cells, 6 to 7 mice). (**D**) Sociability in mice pretreated with one of several dose regimens of the OxtR antagonist (OTRA), L-368,899, before treatment with MDMA or saline. OTRA + saline group is compared to groups receiving MDMA and pretreatment with the following: saline; OTRA (5 mg/kg once); HI (10 mg/kg once); or MULTI (5 mg/kg every 12 hours for 48 hours preceding MDMA; n = 8 to 12). (**E**) Sociability in mice pretreated with saline or OTRA infused into the NAc before intraperitoneal treatment with MDMA or saline. Saline-NAc + MDMA-intraperitoneal is compared to saline-NAc + saline-intraperitoneal and OTRA-NAc + MDMA-intraperitoneal groups. Results with two OTRAs, L-368,899 and L-371,257, are pooled (n = 9 to 13). (**F**) Sociability after saline or MDMA in mice with selective deletion of OxtRs from SERT+ cells (n = 14 to 17). (**G**) Sociability in mice pretreated with saline or the 5-HT1b receptor antagonist, NAS-181, infused into the NAc before intraperitoneal treatment with MDMA (n = 11 to 12). (**H**) Summary time course graph showing the effect of continuous bath application of NAS-181 (20 μM) on MDMA-induced depression of NAc EPSC amplitude. Pooled data from D1 and D2 MSNs are shown. Right, sample traces, as in (B). (**I**) Summary graph of data in (H) (n = 5 to 8 cells, 3 to 5 mice). (**J**) Sociability after increasing doses of the 5-HT–releasing drug d-fenfluramine (FEN: 1, 5, and 10 mg/kg; n = 10 to 16). (**K**) Time course of sociability index after FEN injection (10 mg/kg; n = 11) versus saline (SAL; n = 14). (**L**) Effect of bath application of FEN (10 μM) on the amplitude of EPSCs recorded from NAc MSNs (n = 5, 3 mice). Top right: Sample EPSC traces taken from time points 1 and 2 as shown. Bottom right: Summary graph of FEN-mediated depression of EPSCs. Scale bars, 100 pA, 25 ms in (B) and (H); 200 pA, 25 ms in (L). Data shown are means ± SEM. Significance was determined for each comparison (statistical test): across groups (one-way ANOVA, unmatched) for (D), (E), and (J); between groups (unpaired t test) for (C), (F), (G), and (I); across group time courses (two-way ANOVA, ordinary) for (K); all planned post hoc between-group comparison (t test with Sidak correction for multiple comparisons). *P < 0.05, ***P < 0.001; ns, P > 0.05.

Our choice to test FEN in preclinical assays was motivated by its known mechanism of action, its documented low abuse potential and its current approval for investigational use in humans (*32*). Consistent with the enhancement of sociability by FEN in our experiments, early clinical data suggest that higher doses of FEN have subjective effects reminiscent of MDMA (*33*). FEN has been reported to improve social deficits in children with autism (*34*). However, like MDMA, long-term and/or heavy use of FEN is associated with cardiovascular and neurological toxicity (*1*, *7*, *35*). Furthermore, tolerance to MDMA's acute effects may develop with frequent use

(*36*). Thus, it seems prudent to use these drugs sparingly and infrequently, consistent with recent clinical trial designs for MDMA (*4*). To our knowledge, FEN has not been tested for acute prosocial effects in a therapeutic environment.

Our study has important limitations, chief among them that the interpretation of our data is constrained by our choice of behavioral models. We modeled MDMA-induced social preference on the premise that this behavior reflects some aspects of the formation of therapeutic social bonds in humans. Some investigators suggest that MDMA's clinical efficacy in post-traumatic stress disorder is strongly related to establishing the patient-therapist bond (*4*), although others have presented competing hypotheses, including accelerated extinction of learned fear through nonsocial mechanisms (*37*) and renewing the sensitivity to social reward (*29*). All of these processes may have clinical relevance, and their apparently distinct pharmacological and circuit-based mechanisms could potentially be tested in humans. A further limitation of our work is the incomplete account of how MDMA-induced changes in synaptic strength relate to MDMA-induced behavior. Is MDMA-LTD in the NAc necessary to express prosocial behaviors driven by MDMA? It seems unlikely that LTD of EPSCs in the NAc, a phenomenon associated with behaviors related to mood, addiction, and motivation (*15*, *38*, *39*, *40*), has specificity for prosocial behavior. We speculate that future studies will find that behavioral output strongly depends on which excitatory inputs to the NAc undergo LTD. MDMA's prosocial effect may in part rely on the selective filtering of these inputs.

Given MDMA's long history of abuse and potential toxicity, it would be prudent to develop drugs or other therapies that mimic its prosocial effects with reduced associated morbidities. We propose that future therapeutic strategies, including drug design and brain stimulation approaches, may be more successfully developed by targeting relevant brain circuits rather than by modifying existing drugs based on putative structure/activity relationships. Although much remains unknown about the detailed neural mechanisms by which increased 5-HT release in the NAc promotes sociability, our findings provide a defined mechanistic basis for the further development and testing of agents that positively influence social interactions in a therapeutic manner.

MATERIALS AND METHODS

Study design

For all behavioral tests (three-chamber social approach, locomotion, CPP, and elevated plus maze) experimental groups were interleaved with control groups. Experimental group sizes were determined by power analyses using the effect size observed during initial exploratory experiments, taking into account historical accuracy within our group for stereotactic targeting of a given brain region. All behavioral experiments were conducted in a blind manner such that animals were randomized by cage before surgery and experiments. For experiments involving transgenic animals, the experimenter was blind to the genotype. Performance of a behavioral experiment and analysis of the resulting data were performed by separate individuals, and analysis was performed without knowledge of experimental group assignment.

Animals

Male and female C57BL/6 mice, aged 4 to 16 weeks, (the Jackson Laboratory, stock number 000664), and the following transgenic lines were used:

1) Slc6a4$^{fl/fl}$ (homozygous), Slc6a4$^{fl/wt}$ (heterozygous), and wild-type littermate mice, male and female (SERT$^{fl/fl}$, SERT$^{fl/wt}$, and SERT$^{wt/wt}$, gift from J.-Y. Sze, Albert Einstein College of Medicine) (*41*);

2) Tg(Slc6a4-cre)ET33Gsat male mice (SERT-Cre, GENSAT Project at Rockefeller University; MGI: 3836639) (*42*);

3) B6.129(Cg)-Slc6a4^{tm1Kpl}/J male mice (SERT-KO, the Jackson Laboratory, stock number: 008355)

4) Oxtr$^{tm1.1Wsy}$/J homozygous (OxtR$^{fl/fl}$, the Jackson Laboratory, stock number 008471; MGI:3800791) (*43*);

5) SERT-Cre × OTR$^{fl/fl}$ male mice were generated in the Malenka laboratory using a breeding strategy previously described for producing DAT-Cre × OTR$^{fl/fl}$ mice (*30*).

6) Drd1a–td Tomato/Drd2–enhanced green fluorescent protein (eGFP) bacterial artificial chromosome (BAC) double transgenic mice were backcrossed to wild-type C57BL/6 mice (the Jackson Laboratory, as above), and offspring (*44*) were used for electrophysiology experiments.

For electrophysiology experiments shown in fig. S4, wild-type mice aged 4 to 5 weeks were used. For all other experiments, mice aged 8 to 16 weeks were used. All transgenic mice were maintained on a C57BL/6 background and housed on a 12-hour light/dark cycle with food and water ad libitum. All behavioral experiments were conducted during the same circadian period (7:00 a.m. to 4:00 p.m.). All procedures complied with animal care standards set forth by the National Institute of Health and were approved by Stanford University's Administrative Panel on Laboratory Animal Care and Administrative Panel of Biosafety.

Stereotactic surgery

All surgeries were performed in a sterile, temperature-controlled environment. Mice were anesthetized with inhaled isoflurane (1 to 1.5%), maintaining spontaneous respiration. Mice were positioned in a stereotactic head frame (Kopf Instruments, Model 940), and the skull surface was exposed. Craniotomy for viruses and implants was made with a 0.5-mm drill bit (Fine Science Tools, 19007-05). Implants were stabilized with the insertion of one to two skull screws (Antrin Miniature Specialties; 00-90 × 1/16), and sequential application of C&B Metabond (Parkell) and Dual Cure Resin Ionomer (DenMat, Geristore, no. 4506). Local anesthetic (lidocaine 0.5%, APP Pharmaceuticals LLC) was infiltrated into the scalp incision and meloxicam (Boehringer Ingelheim Vetmedica Inc., 5 mg/kg subcutaneously) was given for postoperative analgesia.

Virus injection

A syringe (Hamilton, Reno, Model 85 RN SYR) with a 33-gauge needle (VWR, no. 7762) was used to infuse 400 nl of virus into the DR [bregma coordinates: anteroposterior (AP) −4.36 mm, mediolateral (ML) 0.00 mm, and dorsoventral (DV) −3.00 mm]. Virus was infused at a rate of 100 nl/min, and the injection needle was withdrawn 5 min after the end of the infusion. Viruses used in this study were purchased from the Stanford Neuroscience Gene Vector and Virus Core and include DJ-AAV-hSyn-Cre-eGFP and DJ-AAV-EF1a-DIO-GCaMP6f. For behavioral experiments involving virus injection, behavior was assessed at least 4 weeks after surgery.

Drug infusion cannula implants

Double-lumen, 26-gauge threaded cannula guides for bilateral drug infusion were custom-ordered (Plastics One). Cannula guides were lowered into the craniotomy sites to a position 1.5 mm above the

target structure. After securing the cannula guide (see above), a bilateral stylet ("dummy cannula") was inserted into the infusion ports, and the device was sealed with a threaded aluminum cap. Cannula guide dimensions were as follows: (NAc infusions) 1.8-mm separation, 8-mm pedestal, cut 3.5 mm below pedestal; (VTA infusion) 1.0-mm separation, 8-mm pedestal, cut 3.8 mm below pedestal. Bregma coordinates for cannula guide implantation were as follows: (NAc) AP +1.50 mm, ML ±0.90 mm, and DV −2.80 mm; (VTA) AP −3.05 mm, ML ±0.50 mm, and DV −3.13 mm. For drug infusion studies, behavioral experiments were performed 2 to 4 weeks after surgery.

Optical fiber implants

Fiber optic implants (Doric Lenses, 400 μm thick, 0.48 numerical aperture, custom-cut to length) for fiber photometry experiments in the NAc were lowered into the craniotomy site and secured, as described above, at bregma coordinates: AP −1.50 mm, ML −0.90 mm, and DV −4.3 mm.

Three-chamber social approach

The three-chamber apparatus was constructed in the laboratory using 0.635-cm-thick sheets of clear extruded acrylic for walls, and Komatex for floors (white) and barrier walls (black; TAP Plastics). The three-chamber apparatus (length × width × height; 72 cm × 23 cm × 25 cm) consisted of two outer chambers (28 cm × 23 cm) connected by a center chamber (16 cm × 23 cm). Translucent acrylic walls with 6.5-cm-diameter holes for mouse passage, drilled 1 cm from the chamber floor, defined the center chamber. These walls were omitted from the fiber photometry experiments to allow for patch cord connection to the free mouse. "Cup mice" were kept in one of two compartments under a 10-cm-diameter inverted metal pencil cup.

All mice were handled daily for three consecutive days, habituated to the behavioral testing room, and habituated to intraperitoneal saline injection before behavioral testing. Social approach testing was performed similar to previously described methods (*17*). On the test day, experimental mice ("free") were habituated to the three-chamber apparatus for 10 min, with an empty inverted wire pencil cup placed in each outer chamber. Mice were briefly returned to their home cage, and after receiving test drug or saline intraperitoneal injections, or an intracerebral infusion, they were replaced into the three-chamber apparatus, now confined to the center chamber by removable opaque barrier walls. A conspecific, age- and sex-matched, wild-type, unfamiliar (noncagemate) mouse was placed under one of the inverted cups (cup mouse). The cup mouse, except in the experiment described in Fig. 1E, received no drug treatment. Fifteen minutes after intraperitoneal injection, dividing walls were removed, and free mice were allowed to explore the entire apparatus for 30 min. At the end of the session, mice were returned to their home cage. Between experimental sessions, cups and the three-chamber apparatus were sprayed with Virkon S and 70% ethanol and wiped down. The cup mouse side of the apparatus and the cups used to hold mice were regularly rotated to minimize the effect of residual scent cues on behavioral testing.

Video was acquired by a computer-controlled ceiling-mounted digital camera and analyzed offline using Biobserve tracking software (Biobserve GmbH). Fidelity of automated mouse tracking was verified for each experiment, and time spent, per minute, was quantified for each of the three chambers. To enable comparisons across treatment groups and minimize the impact of variable exploration times between mice, we calculated a "sociability index" for each mouse as 100 × (cup mouse time − cup time)/(cup mouse time + cup time). Mice were excluded from further analysis if they either failed to explore both cup and cup mouse chambers or if they spent more than 75% of allotted time in the center chamber, not exploring either cup.

For three-chamber social approach experiments, mice were typically used once in an experimental group and once in a control group, with treatments occurring at least 1 week apart to allow for drug washout. We verified that MDMA (7.5 mg/kg) could elicit a similar prosocial effect when given 1 week apart (fig. S1J and table S1).

Locomotor assay

The locomotor testing chamber (Med Associates) was an acrylic box, with internal dimensions of 28 cm by 28 cm by 20 cm. Mice were allowed to explore for 60 min, starting immediately after intraperitoneal injection. Mouse movement was tracked by an array of infrared beam break counters, recorded using Med Associates software, and analyzed offline.

Conditioned place preference

Two equal-sized compartments were created within each locomotor testing chamber described above. Each compartment had a distinct floor, either clear, textured acrylic ("A" side) or smooth, black acrylic ("B" side). Left/right positioning of the floors was alternated between conditioning chambers. Conditioning experiments involving MDMA took place over four consecutive days unless otherwise noted (fig. S2, H and I).

Day 1, pretest

For 30 min, the mouse had free access to both compartments, separated by a clear acrylic divider with a 7-cm-diameter hole for passage. Baseline preference was measured as the amount of time spent per side. Mice were pseudorandomly allocated to either the A or B side for drug conditioning such that net baseline preference within an experimental group was as close to 15.0 min as possible; equal numbers of mice were assigned to A and B sides.

Day 2, first conditioning day

For 60 min, the mouse was sequestered to either A or B side by a solid transparent divider, starting 15 min after receiving test drug or saline treatment. As noted for fig. S2 (H and I), conditioning time was 30 min. For experiments involving intracerebral infusions, any mouse receiving test drug by intracerebral infusion on one conditioning day received intracerebral infusion of saline on the other conditioning day. Half the mice within an experimental group received test drug on day 2 and the other half on day 3.

Day 3, second conditioning day

Experiments are the same as on day 2, with treatment (test drug or saline) and compartment (A or B) switched.

Day 4, post test

Experiments are the same as on day 1.

For METH CPP, two rounds of conditioning were performed, for a total of six consecutive days.

Elevated plus maze

The elevated plus maze consisted of two metal rails (dimensions, 80 cm by 5 cm) perpendicular to each other and intersecting at their centers, as shown in fig. S2D, raised 50 cm above ground level. Opaque black walls (15 cm high) surrounded two arms, whereas the

other arms were open. MDMA (7.5 mg/kg) was given 25 min before a 10-min exploration period. Video was acquired and analyzed as described for the three-chamber assay. Time spent in each arm, number of visits to each arm, and distance traveled were quantified. Comparisons were made for net time and percentage time in the "closed" and "open" arms, and number of visits and percentage of total visits to each arm.

Drug treatments for behavioral experiments

Drugs were administered intraperitoneally at a volume of 0.01 ml/g. MDMA (3 to 15 mg/kg, Sigma-Aldrich), SCIT (7 mg/kg, "escitalopram oxalate," Tocris), METH (2 mg/kg, Sigma-Aldrich), L-368,899 (5 to 10 mg/kg; Tocris), and FEN (1 to 10 mg/kg, Tocris) were all dissolved in 0.9% normal saline. JHW-007 (10 mg/kg, Tocris) was dissolved in 2.5% dimethyl sulfoxide (DMSO) and 0.9% normal saline. For experiments involving two drugs given intraperitoneally, pretreatments (SCIT, L-368,899, JHW-007) were uniformly given 10 min before MDMA intraperitoneal injection.

For intracerebral infusions, all drugs except L-371,257 were dissolved in 0.9% normal saline to achieve a concentration of SCIT (0.5 μg), MDMA (0.5 μg), S(−)-raclopride (+)-tartrate (0.5 μg, Sigma-Aldrich), L-368,899 (0.5 μg), or NAS-181 (0.5 μg, Sigma-Aldrich) in 500 nl of infusate, delivered bilaterally at a rate of 350 nl/min. L-371,257 (0.25 μg, Tocris) was dissolved in 5% DMSO and 0.9% normal saline and infused in the same manner as other drugs. This vehicle solution was infused into the NAc alone or in combination with either intraperitoneal saline or MDMA (7.5 mg/kg) for a portion of the experiments represented in Fig. 4E.

For drug infusion, the dummy cannula was replaced with a bilateral infusion cannula measuring 1.5 mm longer than its corresponding cannula guide. Infusions were delivered by inserting drug-primed bilateral infusers into the implanted cannula guide. Infusers were connected via PE-50 tubing to a 23-gauge needle of a syringe (Hamilton, Model 1701 RN and 7786-01) mounted in a dual-syringe pump (Harvard Apparatus, Model 55-2222). After a 90-s infusion, the infuser was held in place for an additional 30 s, then the "dummy cannula" was reinserted into the cannula guide, and the implant was resealed with an aluminum cap. For experiments involving both intraperitoneal injection and intracerebral infusion, intraperitoneal injection was done just after the infusion.

Fiber photometry

AAV-DJ-DIO-GCaMP6f was injected into the DR, and a fiber optic implant was advanced and secured in the NAc using the same stereotactic coordinates noted above. After allowing 3 to 4 weeks for viral expression, mice were first habituated to the fiber photometry apparatus including attachment of a 2-m patch cord for 30 min and then tested on a subsequent day. Behavior testing consisted of the three-chamber assay, as described above, with continuous video and fiber photometry acquisition. Fiber photometry data were acquired with Synapse software controlling an RZ5P lock-in amplifier (Tucker-Davis Technologies). GCaMP6f excitation was achieved with frequency-modulated 473- and 405-nm light-emitting diodes (Doric), to stimulate Ca^{2+}-dependent and isosbestic emission, respectively. All optical signals were band-pass–filtered with a Fluorescence Mini Cube FMC4 (Doric), emission was measured with a femtowatt photoreceiver (2151; Newport), and signal was digitized at 6 kHz.

Signal processing was performed with MATLAB (MathWorks Inc.). To correct for motion artifact and fluorescent bleaching, signals generated from the two excitation wavelengths (F_{473} and F_{405}) were used to calculate $\Delta F/F = (F_{472} - F_{405})/\text{mean}\,(F_{405})$. For instances where fluorescent decay of F_{473} and F_{405} appeared to have different time constants (that is, F_{473}/F_{405} was markedly nonlinear), each signal F_λ was debleached by fitting with a mono- or biexponential decay function; $\Delta F/F_\lambda$ was calculated for each wavelength as $F_\lambda/\text{mean}(F_\lambda)$; the final corrected $\Delta F/F$ was then calculated as $\Delta F/F_{472} - \Delta F/F_{405}$. For experiments involving quenching of fluorescence by MDMA, corrections were applied using data preceding drug application. A zero-phase digital filter was applied to the resulting signal, and data were z-scored for some comparisons as indicated in main text.

Video for fiber photometry experiments in the three-chamber apparatus was acquired as described above. High-resolution motion tracking was done with TopScan software (CleverSys). Z score or $\Delta F/F$ versus time, and mouse position versus time, were combined to create a map of the maximal z score observed for each position visited by the test mouse within the three-chamber apparatus over a 30-min session. For quantitation of fluorescent signal associated with the mouse cup and "empty cup," maximal z scores were summed for all positions in a 9 cm × 9 cm area centered on the cup. For the illustrated example (Fig. 3I), the maximal z score map was linearly interpolated by a factor of 10 for presentation.

Electrophysiology

Whole-cell recordings were performed in 2- to 4-month-old male mice, either Drd1a–td Tomato/Drd2-eGFP BAC double transgenic mice, or wild-type C57BL/6. For experiments summarized in fig. S4, recordings were performed in 4- to 5-week-old mice. Coronal slices containing the NAc, identified by the corpus callosum and anterior commissure, were prepared as previously described (*15*). Briefly, mice were deeply anesthetized with pentobarbital until unresponsive to tail pinch but still breathing. Ninety-five percent O_2 was supplied by face mask until the left ventricle was cannulated, and the mouse was perfused through this cannula with ice-cold "sucrose solution" containing the following: 215 mM sucrose, 2.5 mM KCl, 20 mM glucose, 26 mM $NaHCO_3$, 1.6 mM NaH_2PO_4, 1 mM $CaCl_2$, 4 mM $MgSO_4$, and 4 mM $MgCl_2$. After brain removal, blocked hemispheres were mounted, and 250-μm-thick slices were cut on a vibratome (Leica, VT1200S) in ice-cold sucrose solution. Slices were immediately transferred to a bath containing artificial cerebrospinal fluid (ACSF), warmed to 35°C, containing the following: 124 mM NaCl, 2.5 mM KCl, 10 mM glucose, 26 mM $NaHCO_3$, 1 mM NaH_2PO_4, 2.5 mM $CaCl_2$, and 1.3 mM $MgSO_4$. After 30 min, slices were maintained at room temperature (RT) for at least 1 hour before transfer to the recording chamber. Cutting and recording solutions were saturated with 95% O_2 and 5% CO_2 (pH 7.4). Experiments were performed at 30.0° ± 0.3°C.

Upon transfer to the recording chamber, slices were completely submerged and continuously superfused at a flow rate of 3 ml/min with ACSF containing the γ-aminobutyric acid type A receptor antagonist, picrotoxin (50 μM, Sigma-Aldrich). A stainless steel monopolar stimulating electrode (2- to 5-megohm impedance, FHC) was advanced into tissue and placed about 150 to 300 μm away from the recording site and near the anterior commissure. Capillary glass pipettes (3 to 4 megohms) were filled with an internal solution containing the following: 130 mM $CsMeSO_3$, 10 mM Hepes, 0.4 mM EGTA, 5 mM tetraethylammonium-chloride, 7 mM Na_2phosphocreatine, 4 mM MgATP, 0.4 mM NaGTP, 0.1 mM spermine, and 4 mM QX-314 Cl (pH 7.3; 290 to 295 mOsm). Neurons were patched under direct

visualization using infrared-filtered differential interference contrast microscopy. Fluorophore-labeled neurons were identified before patching using epifluorescence microscopy. Whole-cell, voltage-clamp recordings were performed with a MultiClamp 700A amplifier (Axon Instruments Inc.) whose output signals were filtered at 3 kHz; recordings were digitized at 20 kHz. After establishing intracellular access, cells were held at −70 mV. Series resistance (typically 8 to 20 megohms) and input resistance (typically 100 to 300 megohms) were continuously monitored throughout each experiment with a −5-mV, 80-ms command pulse delivered before each electrical stimulus pair. Cells with more than 20% change in series resistance were excluded from analysis. Series resistance, input resistance, holding current, and EPSC amplitude were analyzed online using customized software for Igor Pro (WaveMetrics Inc.).

To evoke EPSCs, square pulse stimuli (200-μs pulse width, 50-ms interval) were delivered via a constant-voltage stimulator every 15 s. Stimulation intensity was adjusted to evoke EPSCs with amplitudes of 200 to 500 pA. For each experiment, a baseline (minimum of 10 min) was first obtained in which EPSC amplitude did not vary from beginning to end of baseline period by more than 15%. Test drugs were added from stock solutions, maintained on ice, to the ACSF reservoir at a dilution of 1:1000 to achieve the following concentrations: 10 μM MDMA, 20 μM NAS-181, 10 μM FEN, and 5 μM L-368,899. Stock solution was diluted 1:5000 to achieve 2 μM MDMA. MDMA and FEN were applied for 10 min and then washed out with the ACSF recording solution. NAS-181 was continuously superfused throughout experiments. L-368,899 was applied to slices for at least 30 min before application of MDMA. To quantify the change in EPSC after drug application for experiments shown in Fig. 4 (A to C, H, I, and L), the average EPSC amplitude from 15 to 20 min after drug application (time "0") was calculated. For experiments shown in fig. S4 (A and B), average EPSC amplitude was calculated at peak MDMA effect (10 to 15 min after MDMA) and after MDMA washout (25 to 30 min after MDMA). Representative traces were generated by averaging waveforms from five consecutive minutes of baseline recordings (from 5 min before drug application) or from the postdrug epoch. For presentation, stimulus artifacts were manually removed.

Immunohistochemistry

The animals used in behavioral experiments were terminally anesthetized with pentobarbital, transcardially perfused with 10% formalin, and postfixed overnight in the same solution. The following day, coronal brain sections (60 μM) were cut on a vibratome in 1 M phosphate-buffered saline (PBS) solution. The free-floating sections were permeabilized with PBS–0.3% Triton X-100 for 30 min, incubated for 1 hour at RT in a blocking solution with 5% goat serum in PBS–1% Triton X-100, and then incubated overnight at 4°C with the following primary antibodies (dilution, vendor), in combinations indicated in the text: chicken anti-GFP (1:2000,Aves Labs), rabbit anti-5HT transporter (1:1000, Millipore), and goat anti–tryptophan hydroxylase-2 (TPH-2) (1:1000; Novus). The following day, sections were rinsed in PBS three times for 10 min at RT and incubated in the same blocking solution for 1.5 hours at RT with matched secondary antibodies (1:500; Thermo Fisher Scientific): Alexa Fluor 488 anti-chicken, Alexa Fluor 568 anti-rabbit, and Alexa Fluor 647 anti-goat. The sections were then rinsed three times for 5 min and mounted on slides with 4′,6-diamidino-2-phenylindole Fluoromount-G (SouthernBiotech).

Immunofluorescence quantification

For quantification of anti-SERT immunofluorescence in the DR of AAV-hSyn-Cre-eGFP–injected $SERT^{wt/wt}$ and $SERT^{fl/fl}$ mice (fig. S2), coronal brain slices spanning the DR from these groups of mice were stained as described above with anti-5HT transporter ("anti-SERT") and anti–TPH-2 antibodies. Images were acquired on a Nikon A1 laser scanning confocal microscope at ×10 magnification. Each image was acquired using identical pinhole, gain, offset, and laser settings (1024 × 1024 pixels). Offline analysis using ImageJ was performed for each brain slice in a uniform manner that was blind to mouse genotype as follows: Background subtraction for all images (16-bit) was performed using a rolling ball filter (radius = 50 pixels); region of interest (ROI) defining the DR for each slice was drawn using the anti-TPH2 channel to identify 5-HT neurons; the mean pixel intensity for this ROI in the anti-SERT channel was calculated.

Statistics

Student's two-tailed *t* tests were used to compare two groups. Paired comparisons were performed for CPP assays (before versus after conditioning); unpaired comparisons were used elsewhere. One-way analysis of variance (ANOVA), unmatched, using the Sidak correction for predetermined post hoc subgroup comparisons was used when multiple conditions were compared. Two-way ordinary ANOVA was performed for comparisons of multiple treatment conditions over multiple time points. Statistical analyses were performed using Prism 7.04 (GraphPad Software). All data were tested and shown to exhibit normality and equal variances. All data are expressed as mean ± SEM.

SUPPLEMENTARY MATERIALS

stm.sciencemag.org/cgi/content/full/11/522/eaaw6435/DC1
Fig. S1. Supplementary information supporting data shown in Fig. 1.
Fig. S2. Supplementary information supporting data shown in Fig. 2D.
Fig. S3. Supplementary information supporting data shown in Fig. 3.
Fig. S4. Low-dose MDMA effect on EPSCs in NAc brain slices is not blocked by an OxtR antagonist.
Table S1. Numerical and statistical data supporting Fig. 1 and fig. S1.
Table S2. Numerical and statistical data supporting Fig. 2.
Table S3. Numerical and statistical data supporting Fig. 3.
Table S4. Numerical and statistical data supporting Fig. 4 and fig. S4.
Data file S1. Raw data.

View/request a protocol for this paper from *Bio-protocol*.

REFERENCES AND NOTES

1. U. D. McCann, G. A. Ricaurte, in *The Effects of Drug Abuse on the Human Nervous System*, B. Madras, M. Kuhar, Eds. (Elsevier Inc., 2013), pp. 475–497.
2. G. Greer, R. Tolbert, Subjective reports of the effects of MDMA in a clinical setting. *J. Psychoactive Drugs* **18**, 319–327 (1986).
3. P. Kamilar-Britt, G. Bedi, The prosocial effects of 3,4-methylenedioxymethamphetamine (MDMA): Controlled studies in humans and laboratory animals. *Neurosci. Biobehav. Rev.* **57**, 433–446 (2015).
4. A. A. Feduccia, J. Holland, M. C. Mithoefer, Progress and promise for the MDMA drug development program. *Psychopharmacology* **235**, 561–571 (2018).
5. A. L. Danforth, C. S. Grob, C. Struble, A. A. Feduccia, N. Walker, L. Jerome, B. Yazar-Klosinski, A. Emerson, Reduction in social anxiety after MDMA-assisted psychotherapy with autistic adults: A randomized, double-blind, placebo-controlled pilot study. *Psychopharmacology* **235**, 3137–3148 (2018).
6. A. R. Green, A. O. Mechan, J. M. Elliott, E. O'Shea, M. I. Colado, The pharmacology and clinical pharmacology of 3,4-methylenedioxymethamphetamine (MDMA, "ecstasy"). *Pharmacol. Rev.* **55**, 463–508 (2003).
7. R. B. Rothman, M. H. Baumann, Therapeutic and adverse actions of serotonin transporter substrates. *Pharmacol. Ther.* **95**, 73–88 (2002).

8. H. de Wit, T. J. Phillips, Do initial responses to drugs predict future use or abuse? *Neurosci. Biobehav. Rev.* **36**, 1565–1576 (2012).
9. G. F. Koob, N. D. Volkow, Neurocircuitry of addiction. *Neuropsychopharmacology* **35**, 217–238 (2010).
10. K. A. Brennan, C. Carati, R. A. Lea, P. S. Fitzmaurice, S. Schenk, Effect of D1-like and D2-like receptor antagonists on methamphetamine and 3,4-methylenedioxymethamphetamine self-administration in rats. *Behav. Pharmacol.* **20**, 688–694 (2009).
11. A. Vidal-Infer, C. Roger-Sánchez, M. Daza-Losada, M. A. Aguilar, J. Miñarro, M. Rodríguez-Arias, Role of the dopaminergic system in the acquisition, expression and reinstatement of MDMA-induced conditioned place preference in adolescent mice. *PLOS ONE* **7**, e43107 (2012).
12. M. E. Liechti, F. X. Vollenweider, Which neuroreceptors mediate the subjective effects of MDMA in humans? A summary of mechanistic studies. *Hum. Psychopharmacol.* **16**, 589–598 (2001).
13. A. C. Oakly, B. W. Brox, S. Schenk, B. A. Ellenbroek, A genetic deletion of the serotonin transporter greatly enhances the reinforcing properties of MDMA in rats. *Mol. Psychiatry* **19**, 534–535 (2014).
14. J. M. Trigo, T. Renoir, L. Lanfumey, M. Hamon, K.-P. Lesch, P. Robledo, R. Maldonado, 3,4-methylenedioxymethamphetamine self-administration is abolished in serotonin transporter knockout mice. *Biol. Psychiatry* **62**, 669–679 (2007).
15. G. Dölen, A. Darvishzadeh, K. W. Huang, R. C. Malenka, Social reward requires coordinated activity of nucleus accumbens oxytocin and serotonin. *Nature* **501**, 179–184 (2013).
16. J. J. Walsh, D. J. Christoffel, B. D. Heifets, G. A. Ben-Dor, A. Selimbeyoglu, L. W. Hung, K. Deisseroth, R. C. Malenka, 5-HT release in nucleus accumbens rescues social deficits in mouse autism model. *Nature* **560**, 589–594 (2018).
17. S. S. Moy, J. J. Nadler, A. Perez, R. P. Barbaro, J. M. Johns, T. R. Magnuson, J. Piven, J. N. Crawley, Sociability and preference for social novelty in five inbred strains: An approach to assess autistic-like behavior in mice. *Genes Brain Behav.* **3**, 287–302 (2004).
18. G. Griebel, C. Belzung, G. Perrault, D. J. Sanger, Differences in anxiety-related behaviours and in sensitivity to diazepam in inbred and outbred strains of mice. *Psychopharmacology* **148**, 164–170 (2000).
19. H. Walum, L. J. Young, The neural mechanisms and circuitry of the pair bond. *Nat. Rev. Neurosci.* **19**, 643–654 (2018).
20. G. Rudnick, S. C. Wall, The molecular mechanism of "ecstasy" [3,4-methylenedioxy-methamphetamine (MDMA)]: Serotonin transporters are targets for MDMA-induced serotonin release. *Proc. Natl. Acad. Sci. U.S.A.* **89**, 1817–1821 (1992).
21. G. A. Gudelsky, J. F. Nash, Carrier-mediated release of serotonin by 3,4-methylenedioxymethamphetamine: Implications for serotonin-dopamine interactions. *J. Neurochem.* **66**, 243–249 (1996).
22. Y. Hagino, Y. Takamatsu, H. Yamamoto, T. Iwamura, D. L. Murphy, G. R. Uhl, I. Sora, K. Ikeda, Effects of MDMA on extracellular dopamine and serotonin levels in mice lacking dopamine and/or serotonin transporters. *Curr. Neuropharmacol.* **9**, 91–95 (2011).
23. B. N. Mathur, N. A. Capik, V. A. Alvarez, D. M. Lovinger, Serotonin induces long-term depression at corticostriatal synapses. *J. Neurosci.* **31**, 7402–7411 (2011).
24. H.-w. Shen, Y. Hagino, H. Kobayashi, K. Shinohara-Tanaka, K. Ikeda, H. Yamamoto, T. Yamamoto, K.-P. Lesch, D. L. Murphy, F. S. Hall, G. R. Uhl, I. Sora, Regional differences in extracellular dopamine and serotonin assessed by in vivo microdialysis in mice lacking dopamine and/or serotonin transporters. *Neuropsychopharmacology* **29**, 1790–1799 (2004).
25. J. F. Nash, J. Brodkin, Microdialysis studies on 3,4-methylenedioxymethamphetamine-induced dopamine release: Effect of dopamine uptake inhibitors. *J. Pharmacol. Exp. Ther.* **259**, 820–825 (1991).
26. R. I. Desai, T. A. Kopajtic, M. Koffarnus, A. H. Newman, J. L. Katz, Identification of a dopamine transporter ligand that blocks the stimulant effects of cocaine. *J. Neurosci.* **25**, 1889–1893 (2005).
27. K. T. Beier, E. E. Steinberg, K. E. DeLoach, S. Xie, K. Miyamichi, L. Schwarz, X. J. Gao, E. J. Kremer, R. C. Malenka, L. Luo, Circuit architecture of VTA dopamine neurons revealed by systematic input-output mapping. *Cell* **162**, 622–634 (2015).
28. L. M. Barnett, T. E. Hughes, M. Drobizhev, Deciphering the molecular mechanism responsible for GCaMP6m's Ca^{2+}-dependent change in fluorescence. *PLOS ONE* **12**, e0170934 (2017).
29. R. Nardou, E. M. Lewis, R. Rothhaas, R. Xu, A. Yang, E. Boyden, G. Dölen, Oxytocin-dependent reopening of a social reward learning critical period with MDMA. *Nature* **569**, 116–120 (2019).
30. L. W. Hung, S. Neuner, J. S. Polepalli, K. T. Beier, M. Wright, J. J. Walsh, E. M. Lewis, L. Luo, K. Deisseroth, G. Dolen, R. C. Malenka, Gating of social reward by oxytocin in the ventral tegmental area. *Science* **357**, 1406–1411 (2017).
31. S. Garattini, R. Samanin, *Central Mechanisms of Anorectic Drugs* (Monographs of the Mario Negri Institute for Pharmacological Research, Raven Press, 1978).
32. https://clinicaltrials.gov/ct2/results?term=fenfluramine&cntry=US.
33. J. D. Griffith, J. G. Nutt, D. R. Jasinski, A comparison of fenfluramine and amphetamine in man. *Clin. Pharmacol. Ther.* **18**, 563–570 (1975).
34. M. G. Aman, R. A. Kern, Review of fenfluramine in the treatment of the developmental disabilities. *J. Am. Acad. Child Adolesc. Psychiatry* **28**, 549–565 (1989).
35. S. Bhattacharyya, A. H. Schapira, D. P. Mikhailidis, J. Davar, Drug-induced fibrotic valvular heart disease. *Lancet* **374**, 577–585 (2009).
36. A. C. Parrott, Chronic tolerance to recreational MDMA (3,4-methylenedioxymethamphetamine) or Ecstasy. *J. Psychopharmacol.* **19**, 71–83 (2005).
37. M. B. Young, R. Andero, K. J. Ressler, L. L. Howell, 3,4-Methylenedioxymethamphetamine facilitates fear extinction learning. *Transl. Psychiatry* **5**, e634 (2015).
38. B. K. Lim, K. W. Huang, B. A. Grueter, P. E. Rothwell, R. C. Malenka, Anhedonia requires MC4R-mediated synaptic adaptations in nucleus accumbens. *Nature* **487**, 183–189 (2012).
39. N. Schwartz, P. Temkin, S. Jurado, B. K. Lim, B. D. Heifets, J. S. Polepalli, R. C. Malenka, Decreased motivation during chronic pain requires long-term depression in the nucleus accumbens. *Science* **345**, 535–542 (2014).
40. C. Luscher, R. C. Malenka, Drug-evoked synaptic plasticity in addiction: From molecular changes to circuit remodeling. *Neuron* **69**, 650–663 (2011).
41. X. Chen, R. Ye, J. J. Gargus, R. D. Blakely, K. Dobrenis, J. Y. Sze, Disruption of transient serotonin accumulation by non-serotonin-producing neurons impairs cortical map development. *Cell Rep.* **10**, 346–358 (2015).
42. S. Gong, M. Doughty, C. R. Harbaugh, A. Cummins, M. E. Hatten, N. Heintz, C. R. Gerfen, Targeting Cre recombinase to specific neuron populations with bacterial artificial chromosome constructs. *J. Neurosci.* **27**, 9817–9823 (2007).
43. H. J. Lee, H. K. Caldwell, A. H. Macbeth, S. G. Tolu, W. S. Young III, A conditional knockout mouse line of the oxytocin receptor. *Endocrinology* **149**, 3256–3263 (2008).
44. A. B. Nelson, G. B. Hang, B. A. Grueter, V. Pascoli, C. Luscher, R. C. Malenka, A. C. Kreitzer, A comparison of striatal-dependent behaviors in wild-type and hemizygous Drd1a and Drd2 BAC transgenic mice. *J. Neurosci.* **32**, 9119–9123 (2012).

Acknowledgments: We thank J. Pollepali, K. Beier, M. Pavlovic, M.A. Wright, and R. de Gregorio for technical assistance. **Funding:** This work was supported by grants from the Wu Tsai Neurosciences Institute and NIH P50 DA042012 (to R.C.M.), K08 MH110610 (to B.D.H.), F32 MH115668 (to P.H.), and MH105839 (to J.Y.S.). **Author contributions:** B.D.H. and R.C.M. initiated the project and designed the experiments. B.D.H., J.S.S., M.D.T., D.F.C.P., E.E.S., and J.J.W. performed and analyzed behavioral assays. B.D.H. performed and analyzed fiber photometry assays. B.D.H. and P.H. performed and analyzed electrophysiological assays. J.Y.S. generated and helped characterize $SERT^{fl/fl}$ mice. B.D.H. and R.C.M. wrote the paper, which was reviewed, edited, and approved by all authors. **Competing interests:** R.C.M. is on the scientific advisory boards of MapLight Therapeutics Inc., Cerevance, Cognition Therapeutics Inc., and the Brave Neuroscience Company. **Data and materials availability:** All data associated with this study are present in the paper or the Supplementary Materials.

Submitted 11 January 2019
Resubmitted 1 August 2019
Accepted 15 October 2019
Published 11 December 2019
10.1126/scitranslmed.aaw6435

Citation: B. D. Heifets, J. S. Salgado, M. D. Taylor, P. Hoerbelt, D. F. Cardozo Pinto, E. E. Steinberg, J. J. Walsh, J. Y. Sze, R. C. Malenka, Distinct neural mechanisms for the prosocial and rewarding properties of MDMA. *Sci. Transl. Med.* **11**, eaaw6435 (2019).

Science Translational Medicine

Distinct neural mechanisms for the prosocial and rewarding properties of MDMA

Boris D. Heifets, Juliana S. Salgado, Madison D. Taylor, Paul Hoerbelt, Daniel F. Cardozo Pinto, Elizabeth E. Steinberg, Jessica J. Walsh, Ji Y. Sze and Robert C. Malenka

Sci Transl Med **11**, eaaw6435.
DOI: 10.1126/scitranslmed.aaw6435

Dissecting MDMA

MDMA, commonly known as ecstasy, is a psychoactive drug primarily used for recreational purposes. Because of its prosocial effects, MDMA is currently being evaluated for the treatment of psychiatric disorders. Unfortunately, the rewarding addictive properties hinder the therapeutic use. Now, Heifets *et al.* investigated the mechanisms mediating the effects of MDMA in rodents and found that the prosocial and the rewarding effects are mediated by independent mechanisms. The prosocial effects are mediated by activation of the serotoninergic system, whereas the rewarding effect requires the activation of the dopaminergic signaling. The results pave the way for the development of more specific therapeutic intervention with less side effects.

Science Translational Medicine (ISSN 1946-6242) is published by the American Association for the Advancement of Science, 1200 New York Avenue NW, Washington, DC 20005. The title *Science Translational Medicine* is a registered trademark of AAAS.

Science Translational Medicine
AAAS

stm.sciencemag.org/cgi/content/full/11/522/eaaw6435/DC1

Supplementary Materials for

Distinct neural mechanisms for the prosocial and rewarding properties of MDMA

Boris D. Heifets, Juliana S. Salgado, Madison D. Taylor, Paul Hoerbelt, Daniel F. Cardozo Pinto, Elizabeth E. Steinberg, Jessica J. Walsh, Ji Y. Sze, Robert C. Malenka*

*Corresponding author. Email: malenka@stanford.edu

Published 11 December 2019, *Sci. Transl. Med.* **11**, eaaw6435 (2019)
DOI: 10.1126/scitranslmed.aaw6435

The PDF file includes:

Other Supplementary Material for this manuscript includes the following:

(available at stm.sciencemag.org/cgi/content/full/11/522/eaaw6435/DC1)

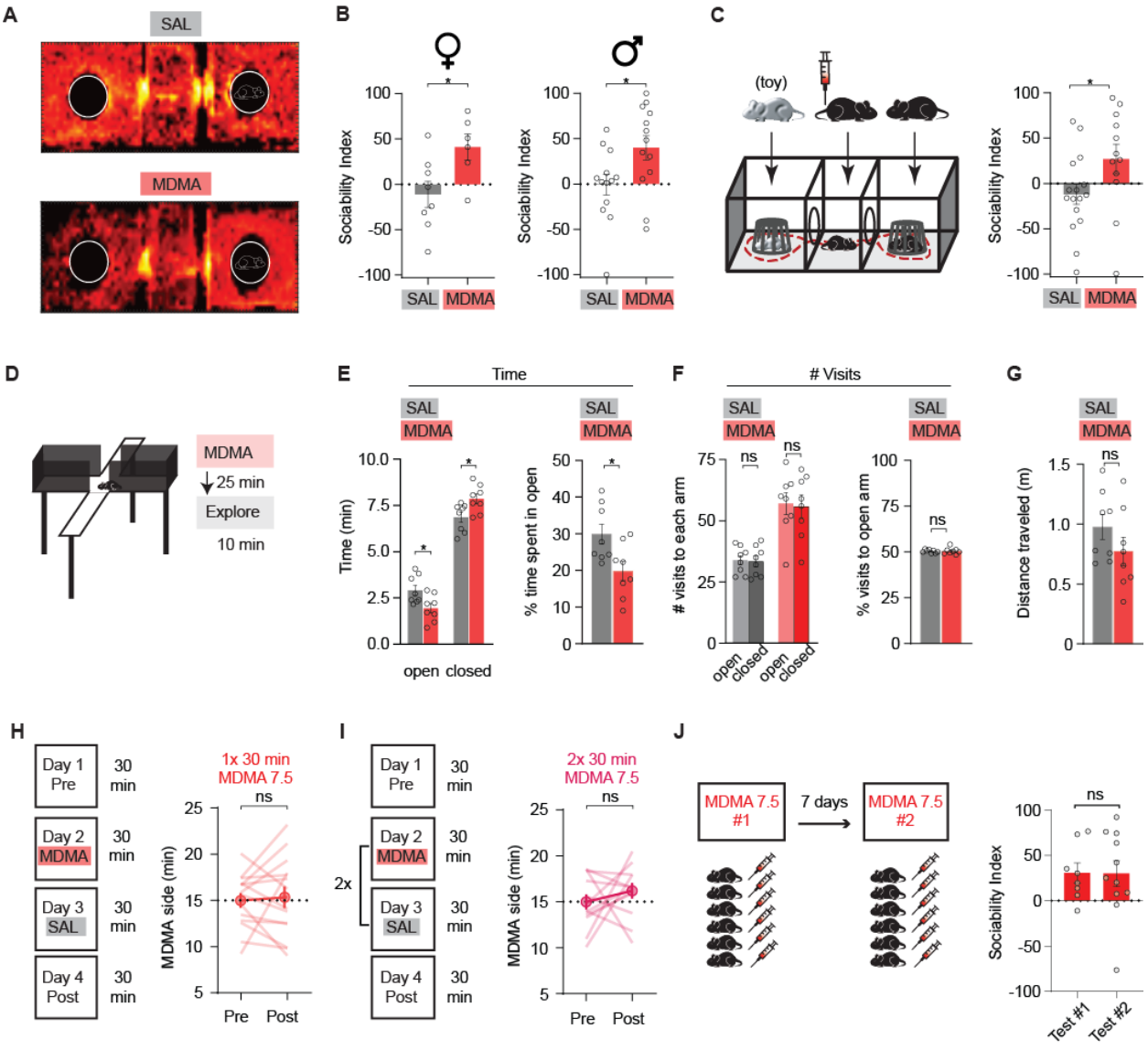

Fig. S1. Supplementary information supporting data shown in Fig. 1. (A) Sample heat map illustrating the relative amounts of time, which a saline- or MDMA-treated mouse spent within each position of the three-chamber testing apparatus over the 30-minute exploration period. Heat map construction: the sum total of visits to each square centimeter was calculated; for visualization, the map (M) was transformed by 1 + log(M); map was interpolated by a factor of 10; a gaussian smoothing function was applied. **(B)** Sociability after MDMA (7.5 mg/kg) in adult female mice (*left*; N=6-8) and adult male mice (*right*; N=13). **(C)** Sociability after MDMA (7.5 mg/kg) when an unfamiliar toy mouse (schematic at *left*) is placed in the empty cup (summary graph at *right*; N=12-16). **(D)** Schematic of elevated-plus maze and experimental time line. **(E)** Time spent in the open-arm areas after either MDMA (7.5 mg/kg) or saline treatment, as measured by total time and % of total time (N=8). **(F)** Same experiment as **(E)**, quantifying the

visits made to each arm as total number and % of total visits. **(G)** Same experiment as **(E)**, distance traveled after MDMA (7.5 mg/kg) compared to saline. **(H)** CPP data after a shorter duration of pairing MDMA 7.5 mg/kg with a unique context (30 min versus the 1 hr shown in **Fig. 1H**; N=14). **(I)** CPP data after two pairings of MDMA 7.5 mg/kg with a unique context (30 min each; N=12). **(J)** Sociability in the same cohort of mice given two separate doses of MDMA 7.5 mg/kg one week apart (N=12 mice in cohort; Day 0, N=8 and Day 7, N=11 mice meeting criteria for measurement). Data shown are means ± s.e.m. Significance was determined between groups using an unpaired t-test for (B), (C), (E), (F, *right*), (G), (J); within group (paired t-test) for (F, *left*), (H), (I). *P<0.05.

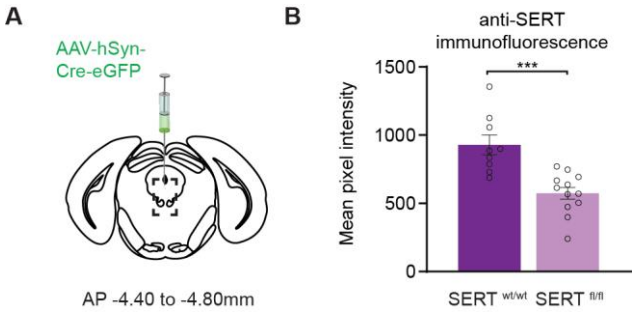

Fig. S2. Supplementary information supporting data shown in Fig. 2D. (A) Schematic drawing of DR injected with AAV-Cre, denoting approximate range of antero-posterior position for slices used to quantify anti-SERT immunofluorescence. **(B)** Anti-SERT immunofluorescence intensity quantification in DR of AAV-Cre injected $SERT^{wt/wt}$ and $SERT^{fl/fl}$ mice. Data shown are means ± s.e.m. Significance was determined between groups (unpaired t-test) for (B). ***P<0.001.

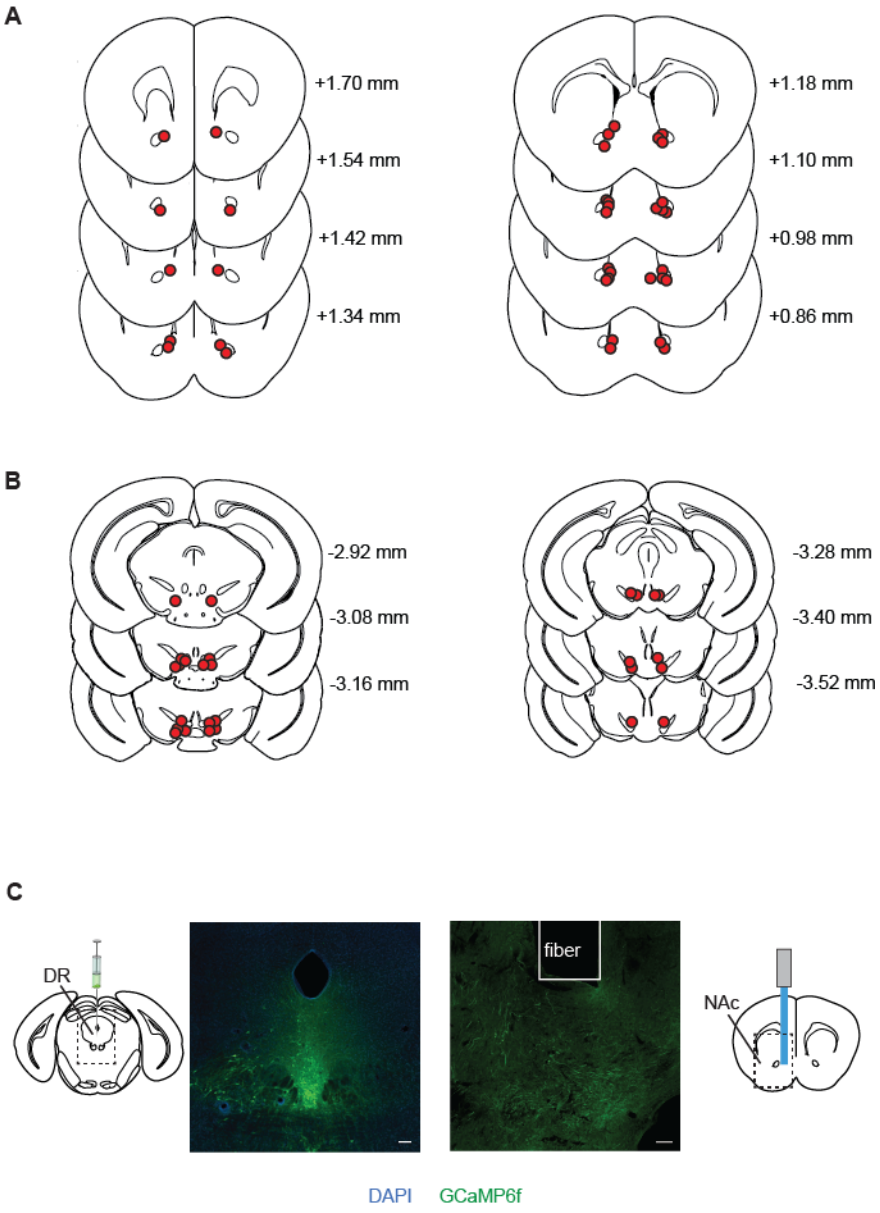

Fig. S3. Supplementary information supporting data shown in Fig. 3. (A and **B)** Location of infuser tips of cannulae implanted for intra-NAc drug delivery **(A; Fig. 3A, C, D)**, and intra-VTA drug delivery **(B; Fig. 3B)**. **(C)** Sample images showing virus injection (DJ-AAV-EF1a-DIO-GCaMP6f) into the DR of SERT-Cre mice *(left)* and optical fiber placement in the NAc *(right)*, for fiber photometry experiments **(Fig. 3E-L)**. GCaMP6f, green; DAPI, blue. Scale bar = 100 μm.

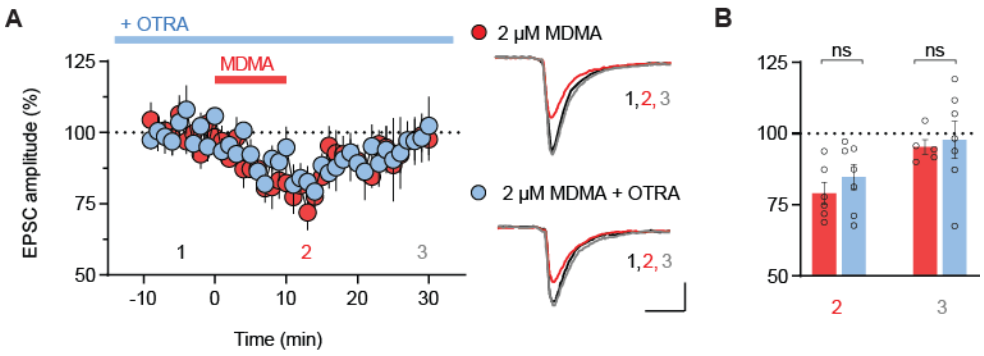

Fig. S4. Low-dose MDMA effect on EPSCs in NAc brain slices is not blocked by an OxtR antagonist. (A) *Left*, Summary timecourse graph showing the effect of a 10 minute bath application of MDMA (2 µM) on EPSC amplitude evoked in NAc MSNs, with and without incubation and continuous application of an OxtR antagonist, L-368,899 (5 µM;N=6-7 cells, 6 mice). *Right*, Sample EPSC traces taken from time points indicated: 1, baseline; 2, peak MDMA effect (10-15 min post infusion); 3, MDMA washout (25-30 min post infusion). Second stimulated EPSCs are omitted for clarity. Scale bars: 100 pA, 10 ms. **(B)** Summary graph of data in **A**, showing EPSC amplitudes at time points 2 and 3 for the 2µM MDMA versus the 2µM MDMA + OTRA groups. Data shown are means ± s.e.m. Significance was determined between groups (unpaired t-test) for (B). ns, P>0.05.

Table S1. Numerical and statistical data supporting Fig. 1 and fig. S1. [a] Planned *post hoc* comparisons performed using Sidak correction for multiple comparisons.

Panel	Group	N	Mean ± SEM (unit)	Primary Statistic	*Post hoc* test[a]
1B	SAL	13	empty, 11.92 ± 0.98 (min) mouse, 12.51 ± 1.10 (min)	One-way ANOVA, unmatched; $F_{7,82}$=6.20, P<0.0001	ns
	MDMA 3 mg/kg	9	empty, 7.76 ± 1.29 (min) mouse, 11.92 ± 1.67 (min)		ns
	MDMA 7.5 mg/kg	13	empty, 7.17 ± 1.13 (min) mouse, 16.21 ± 1.72 (min)		P<0.0001
	MDMA 15 mg/kg	10	empty, 7.94 ± 1.52 (min) mouse, 15.86 ± 1.98 (min)		P=0.0015
1C	SAL	16		Two-way ANOVA, ordinary; Treatment: $F_{1,163}$ = 8.42, P=0.0042 Time: ns	
	MDMA 7.5 mg/kg	14			
1D	SAL	16	-6.31 ± 7.69 (soc. ind.)	Unpaired t-test; P=0.022	
	MDMA 7.5 mg/kg	13	24.49 ± 10.42 (soc. ind.)		
1E	SAL, both mice	12	-2.49 ± 11.26 (soc. ind.)	One-way ANOVA, unmatched; $F_{3,61}$=5.87, P=0.0014	---
	MDMA,	18	14.75 ± 5.14 (soc. ind.)		*vs* SAL, ns
	MDMA, free mouse	20	26.55 ± 7.25 (soc. ind.)		*vs* SAL, P=0.023
	MDMA, both mice	15	42.30 ± 5.42 (soc. ind.)		*vs* SAL, P=0.0005
1F	SAL	10	2.12 ± .33 (m)	One-way ANOVA, unmatched; $F_{3,38}$=9.14, P=0.0001	---
	MDMA 7.5 mg/kg	10	2.18 ± .56 (m)		*vs* SAL, ns
	MDMA 15 mg/kg	11	5.79 ± .65 (m)		*vs* SAL, P=0.0002
1H	MDMA 7.5 mg/kg	10	pre, 15.96 ± 1.02 post, 15.75 ± 1.47	Paired t-test; ns	
	MDMA 15 mg/kg	11	pre 14.66 ± 1.45 post, 18.08 ± 1.43	Paired t-test; P=0.012	
S1B	Female SAL	8	-11.10 ± 14.38 (soc. ind.)	Unpaired t-test; P=0.027	
	Female MDMA 7.5 mg/kg	6	41.15 ± 14.36 (soc. ind.)		
	Male SAL	13	-0.70 ± 11.26 (soc. ind.)	Unpaired t-test; P=0.027	
	Male MDMA 7.5 mg/kg	13	40.14 ± 13.23 (soc. ind.)		
S1C	SAL	16	-11.96 ± 10.99 (soc. ind.)	Unpaired t-test; P=0.049	
	MDMA	12	27.01 ± 16.17 (soc. ind.)		
S1E	Open arm, SAL	8	2.93 ± 0.27 (min)	Unpaired t-test; P=0.020	
	Open arm, MDMA 7.5 mg/kg	8	1.95 ± 0.26 (min)		
	Closed arm, SAL		6.87 ± 0.27 (min)	Unpaired t-test; P=0.020	
	Closed arm, MDMA 7.5 mg/kg		7.86 ± 0.26 (min)		
	Open arm, SAL		29.89 ± 2.76 (% total time)	Unpaired t-test; P=0.020	
	Open arm, MDMA 7.5 mg/kg		19.88 ± 2.63 (% total time)		
S1F	Open arm, SAL	8	33.88 ± 1.95 (# visits)	Paired t-test; ns	
	Closed arm, SAL		33.38 ± 2.15 (# visits)		
	Open arm, MDMA 7.5 mg/kg	8	57.00 ± 4.46 (# visits)	Paired t-test; ns	
	Closed arm, MDMA 7.5 mg/kg		55.88 ± 4.60 (# visits)		
	Open arm, SAL		50.44 ± 0.32 (% total visits)	Unpaired t-test;	

	Open arm, MDMA 7.5 mg/kg		50.53 ± 0.61 (% total visits)	ns	
S1G	SAL	8	9.78 ± 1.04 (m)	Unpaired t-test;	
	MDMA 7.5 mg/kg	8	7.75 ± 1.18(m)	ns	
S1H	MDMA 7.5 mg/kg, 30 min x 1	14	pre, 14.98 ± 0.79 post, 15.33 ± 1.17	Paired t-test; ns	
S1I	MDMA 7.5 mg/kg, 30 min x 2	12	pre 14.91 ± 0.82 post, 16.11 ± 0.83	Paired t-test; ns	
S1J	Day 0 MDMA 7.5 mg/kg	8	30.53 ± 10.93 (soc. ind.)	Unpaired t-test;	
	Day 7 MDMA 7.5 mg/kg	11	29.92 ± 14.37 (soc. ind.)	ns	

Table S2. Numerical and statistical data supporting Fig. 2. [a] Planned *post hoc* comparisons performed using Sidak correction for multiple comparisons.

Panel	Group	N	Mean ± SEM (unit)	Primary Statistic	*Post hoc* test[a]
2A	SCIT + SAL	8	3.02 ± 12.78 (soc. ind.)	One-way ANOVA, unmatched; $F_{2,20}$=4.55, P=0.0235	*vs* SAL + MDMA 7.5 mg/kg, P=0.048
	SAL + MDMA 7.5 mg/kg	9	42.41 ± 10.70 (soc. ind.)		---
	SCIT + MDMA 7.5 mg/kg	6	-4.25 ± 12.59 (soc. ind.)		*vs* SAL + MDMA 7.5 mg/kg, P<0.030
2E	$SERT^{wt/wt}$ SAL	22	1.56 ± 9.78 (soc. ind.)	Unpaired t-test; P=0.0037	
	MDMA 7.5 mg/kg	14	54.80 ± 14.89 (soc. ind.)		
	$SERT^{wt/fl}$ SAL	17	13.24 ± 11.17 (soc. ind.)	Unpaired t-test; ns	
	MDMA 7.5 mg/kg	16	5.21 ± 17.37 (soc. ind.)		
	$SERT^{fl/fl}$ SAL	8	32.73 ±12.54 (soc. ind.)	Unpaired t-test; P=0.034	
	MDMA 7.5 mg/kg	14	-28.85 ± 19.00 (soc. ind.)		
2F	$SERT^{wt/wt}$ MDMA 15 mg/kg	10	Pre, 14.70 ± 0.73 (min) Post, 17.14 ± 1.09 (min)	Paired t-test; P=0.038	
	$SERT^{wt/fl}$ MDMA 15 mg/kg	22	Pre, 15.43 ± 0.36 (min) Post, 17.47 ± 0.93 (min)	Paired t-test; P=0.033	
	$SERT^{fl/fl}$ MDMA 15 mg/kg	11	Pre, 14.75 ± 0.70 (min) Post, 16.53 ± 1.02 (min)	Paired t-test; P=0.049	
2G	SAL + SAL	15	-16.11 ± 13.61 (soc. ind.)	One-way ANOVA, unmatched; $F_{2,30}$=6.32, P=0.0051	*vs* JHW + MDMA 7.5 mg/kg, P=0.0084
	JHW + MDMA 7.5 mg/kg	8	53.33 ± 15.06 (soc. ind.)		---
	JHW + SAL	10	-25.85 ± 17.33 (soc. ind.)		*vs* JHW + MDMA 7.5 mg/kg, P=0.0055
2H	SAL	10		Two-way ANOVA, ordinary; Treatment: $F_{1,163}$ = 8.42, P=0.029 Time: ns	
	METH 2 mg/kg	9			
2I	SAL, Day 0	8	2.96 ± 0.27 (m)	One-way ANOVA, repeated measures; $F_{3,21}$=50.96, P<0.0001	*vs* METH 2mg/kg Day 1, P=0.0010
	METH 2 mg/kg, Day 1		6.90 ± 0.71 (m)		---
	METH 2 mg/kg, Day 2		12.29 ± 1.06 (m)		---
	METH 2 mg/kg, Day 3		13.30 ± 1.06 (m)		*vs* METH 2mg/kg Day 1, P<0.00001
2J	METH 2 mg/kg	12	Pre, 14.08 ± 1.54 (min) Post, 16.80 ± 1.05 (min)	Paired t-test; P=0.041	
S2B	$SERT^{wt/wt}$ (4 mice)	9	929.6 ± 71.3 (intensity)	Unpaired t-test; P=0.0003	
	$SERT^{fl/fl}$ (6 mice)	12	574.2 ± 44.0 (intensity)		

Table S3. Numerical and statistical data supporting Fig. 3. [a] Planned *post hoc* comparisons performed using Sidak correction for multiple comparisons.

Panel	Group	N	Mean ± SEM (unit)	Primary Statistic	*Post hoc* test[a]
3A	Intra-NAc SCIT + SAL i.p.	20	11.54 ± 7.91 (soc. ind.)	One-way ANOVA, unmatched; $F_{2,51}$=3.36, P=0.043	*vs* Intra-NAc SAL + MDMA 7.5 mg/kg i.p., ns
	Intra-NAc SAL + MDMA 7.5 mg/kg i.p.	15	34.71 ± 13.94 (soc. ind.)		---
	Intra-NAc SCIT + MDMA 7.5 mg/kg i.p.	19	-6.52 ± 11.28 (soc. ind.)		*vs* Intra-NAc SAL + MDMA 7.5 mg/kg i.p., P=0.025
3B	Intra-VTA SCIT + SAL i.p.	18	-7.52 ± 9.01 (soc. ind.)	One-way ANOVA, unmatched; $F_{2,41}$=7.08, P=0.0023	*vs* Intra-VTA SAL + MDMA 7.5 mg/kg i.p., P=0.0042
	Intra-VTA SAL + MDMA 7.5 mg/kg i.p.	13	38.92 ± 10.38 (soc. ind.)		---
	Intra-VTA SCIT + MDMA 7.5 mg/kg i.p.	13	35.67 ± 11.42 (soc. ind.)		*vs* Intra-VTA SAL + MDMA 7.5 mg/kg i.p., ns
3C	Intra-NAc SAL + MDMA 7.5 mg/kg i.p.	13	40.14 ± 13.23 (soc. ind.)	One-way ANOVA, unmatched; $F_{2,33}$=7.89, P=0.0016	*vs* Intra-NAc SAL + SAL i.p., P=0.014
	Intra-NAc SAL + SAL i.p.	11	-1.27 ± 10.12 (soc. ind.)		---
	Intra-NAc MDMA + SAL i.p.	12	55.70 ± 4.56 (soc. ind.)		*vs* Intra-NAc SAL + SAL i.p., P=0.0010
3D	Intra-NAc SAL + MDMA 15 mg/kg i.p.	16	Pre, 14.82 ± 0.65 (min) Post, 17.17 ± 0.72 (min)	Paired t-test; P=0.012	
	Intra-NAc SCIT + MDMA 15 mg/kg i.p.	16	Pre, 15.00 ± 0.44 (min) Post, 18.45 ± 1.03 (min)	Paired t-test; P=0.0015	
	Intra-NAc RAC + MDMA 15 mg/kg i.p.	13	Pre, 14.86 ± 0.98 (min) Post, 15.13 ± 1.16 (min)	Paired –test; ns	
3G	SAL	3	94.21 ± 0.39 (% baseline std. dev.)	Unpaired t-test; P<0.0001	
	MDMA 7.5 mg/kg	3	21.74 ± 4.46 (% baseline std. dev.)		
3K	SERT-Cre, + GCaMP6f	5	Mouse, 2140.0 ± 445.3 (cum. z) Empty, 941.9 ± 263.4 (cum. z)	Unpaired t-test; P=0.049	
3L	SERT-Cre, + GCaMP6f	5	Slope = 0.22 ± 0.057; Y-intercept, 1.77 ± 0.41; X-intercept, -5.40	Linear regression; $F_{1,3}$=14.73, P=0.031	

Table S4. Numerical and statistical data supporting Fig. 4 and fig. S4. [a] Planned *post hoc* comparisons performed using Sidak correction for multiple comparisons.

Panel	Group	N	Mean ± SEM (unit)	Primary Statistic	*Post hoc* test[a]
4C	D1 MSN (7 mice)	8	72.78 ± 7.98 (% baseline EPSC)	Unpaired t-test, ns	
	D2 MSN (6 mice)	7	65.84 ± 5.84 (% baseline EPSC)		
4D	OTRA + SAL	8	-13.95 ± 9.84 (soc. ind.)	One-way ANOVA, unmatched; $F_{4,43}$=3.11, P=0.025	---
	SAL + MDMA 7.5 mg/kg	12	32.88 ± 11.10 (soc. ind.)		*vs* OTRA+ SAL, P=0.031
	OTRA + MDMA 7.5 mg/kg	12	30.70 ± 11.51 (soc. ind.)		*vs* OTRA + SAL, P=0.042
	OTRA high dose + MDMA 7.5 mg/kg	8	34.24 ± 10.61 (soc. ind.)		*vs* OTRA + SAL, P=0.046
	OTRA multiple dose + MDMA 7.5 mg/kg	8	46.45 ± 16.23 (soc. ind.)		*vs* OTRA + SAL, P=0.0086
4E	Intra-NAc SAL + SAL i.p.	11	-10.65 ± 11.69 (soc. ind.)	One-way ANOVA, unmatched; $F_{3,35}$=7.85, P=0.0004	---
	Intra-NAc SAL + MDMA 7.5 mg/kg i.p.	13	39.06 ± 11.23 (soc. ind.)		*vs* Intra-NAc SAL + SAL i.p., P=0.024
	Intra-NAc OTRA + MDMA 7.5 mg/kg i.p.	9	74.31 ± 12.36 (soc. ind.)		*vs* Intra-NAc SAL + SAL i.p., P=0.0003
4F	SAL	17	-2.39 ± 11.78 (soc. ind.)	Unpaired t-test; P=0.048	
	MDMA 7.5 mg/kg	14	33.29 ± 12.51 (soc. ind.)		
4G	Intra-NAc SAL + MDMA 7.5 mg/kg i.p.	12	32.84 ± 15.38 (soc. ind.)	Unpaired t-test, P=0.035	
	Intra-NAc NAS-181 + MDMA 7.5 mg/kg i.p.	11	-17.72 ± 16.43 (soc. ind.)		
4I	MDMA (5 mice)	8	70.10 ± 6.92 (% baseline EPSC)	Unpaired t-test, P=0.0087	
	NAS-181 (3 mice)	5	101.42 ± 5.44 (% baseline EPSC)		
4J	SAL	16	-2.69 ± 10.77 (soc. ind.)	One-way ANOVA, unmatched; $F_{3,46}$=3.43, P=0.025	---
	FEN 1 mg/kg	10	7.41 ± 4.01 (soc. ind.)		*vs* SAL, ns
	FEN 5 mg/kg	13	29.69 ± 8.27 (soc. ind.)		*vs* SAL, P=0.048
	FEN 10 mg/kg	11	34.42 ± 12.04 (soc. ind.)		*vs* SAL, P=0.027
4K	SAL	14		Two-way ANOVA, ordinary; Treatment: $F_{1,138}$=19.76, P<0.0001. Time: ns	
	FEN 10	11			
4L	FEN (3 mice)	5	69.35 ± 4.93 (% baseline EPSC)		
S4B	Time 2 MDMA (6 mice)	6	79.07 ± 3.92 (% baseline EPSC)	Unpaired t-test, ns	
	MDMA + OTRA (6 mice)	7	84.76 ± 4.45 (% baseline EPSC)		
	Time 3 MDMA (5 mice)	5	95.30 ± 2.52 (% baseline EPSC)	Unpaired t-test, ns	
	MDMA + OTRA (6 mice)	7	97.82 ± 6.50 (% baseline EPSC)		